Nature of the excited states of He_2 †

Steven L. Guberman* and William A. Goddard III
Arthur Amos Noyes Laboratory of Chemical Physics, California Institute of Technology, Pasadena, California 91125
(Received 5 August 1974)

The low-lying excited states of He_2 have been examined using spatially projected generalized-valence-bond wave functions. Typically the excited-state potential curves are repulsive at large R (internuclear distance) but exhibit an attractive well at small R. We find that the repulsion at large R results from an unfavorable exchange interaction of a Rydberg orbital mostly on one He with the two core orbitals on the other He. This arises from the restrictions on the molecular wave function implicit in the Pauli principle and is similar in nature to the repulsive pair-pair interactions between ground state He atoms. For $R < 3a_0$ the Rydberg orbital is large compared with R and the shape of the potential curve is determined by core-core interactions. For the $A\ ^1\Sigma_u^+$ state, the calculated maximum in the potential curve is 0.0607 eV at 3.09 Å, in excellent agreement with experimentally derived values. Results are presented for several other excited states.

I. INTRODUCTION

Although the ground states of rare gas diatomic molecules have very small binding energies (~0.001 eV for He_2[1a]; ~0.02 eV for Kr_2[1b]) arising from van der Waals interactions, it is known that the excited states are often strongly bound (by up to about[2] 2.5 eV) although highly excited (e.g., greater than ~15.5 eV for He_2).[3] The combination of high-lying bound excited states and a dissociative ground state suggests several important applications. Since these molecular excited states are generated in rare gas discharges one can use the continuum emissions from these states as light sources in the vacuum ultraviolet.[4] The possibility of using the dissociative ground state to obtain population inversions has caused recent interest to focus on the construction of a far-ultraviolet laser[5] for use in many areas, including application as an initiator of controlled-fusion reactions.[6] Investigations of liquid helium have shown that bombardment with high-energy (i.e., greater than 100 keV) electrons leads to the efficient production of excited states of both He and He_2.[7] Calculations[8] on the excited atoms show that each of these states is apparently inside a bubble more than 10 Å in diam and gives rise to liquid spectra which are remarkably similar to the gas phase spectra. The dense nature of the medium may be important in the development of uv rare gas lasers since it allows for a high concentration of excited states. Lastly, we note that because of their relative simplicity and abundance, the lighter rare gases enable the comparison of experimental and theoretical descriptions of collision processes.[9,10]

A hindrance to these developments has been the lack of an effective theoretical framework for understanding the nature of the electronic interactions characterizing the excited states of the rare gas molecules. For example, it is important to be able to predict the shapes of potential surfaces and discuss in particular (a) which states have maxima on these surfaces, (b) the magnitude of the maxima and their location, (c) which states will be quenched in dense media, (d) which states are strongly bound, and (e) which can predissociate to yield translationally hot excited atoms. In order to consider such problems one needs to have a firm theoretical understanding of the states involved.

Herein we describe results from *ab initio* studies of those excited states of He_2 that dissociate to a ground-state atom plus an excited atom in the $(1s, ns)\,^1S$, $(1s, np)\,^1P$, and $(1s, 3d)\,^1D$ states for $n = 2, 3$. These results are interpreted in terms of qualitative ideas based on the nature of the excited atom involved. In particular we show that the shapes of the potential curves can be understood in terms of interactions between core orbitals and between core and Rydberg orbitals. The latter interaction is shown to be due to the Pauli principle and can be understood simply in terms of the shape of the Rydberg orbital.

II. WAVE FUNCTIONS

In order to understand the approach it will first be necessary to consider wave functions for the He atom before examining the wave functions used to obtain the potential energy curves of He_2. Here we will see that it is necessary to depart somewhat from the Hartree-Fock description.

A. Generalized-valence-bond wave functions for the He atom

The Hartree-Fock (HF) description of the ground and lower excited states of the He atom is shown below:

$$1\,^1S\text{:}\ \phi_{1s}\phi_{1s}(\alpha\beta-\beta\alpha), \tag{1}$$

$$2\,^3S\text{:}\ (\phi_{1\bar{s}}\phi_{2s}-\phi_{2s}\phi_{1\bar{s}})(\alpha\beta+\beta\alpha), \tag{2}$$

$$2\,^1S\text{:}\ (\phi_{1\bar{s}}\phi_{2s}+\phi_{2s}\phi_{1\bar{s}})(\alpha\beta-\beta\alpha), \tag{3}$$

$$2\,^3P\text{:}\ (\phi_{1\bar{s}}\phi_{2p}-\phi_{2p}\phi_{1\bar{s}})(\alpha\beta+\beta\alpha), \tag{4}$$

$$2\,^1P\text{:}\ (\phi_{1\bar{s}}\phi_{2p}+\phi_{2p}\phi_{1\bar{s}})(\alpha\beta-\beta\alpha), \tag{5}$$

where, for example, by $(\phi_{1s}\phi_{2s}+\phi_{2s}\phi_{1s})$ we mean $[\phi_{1s}(1)\phi_{2s}(2)+\phi_{2s}(1)\phi_{1s}(2)]$, and α and β are spin functions. In the HF method each orbital in (1)–(5) is solved for self-consistently so that the $\phi_{1\bar{s}}$ orbitals change slightly as we go from state to state. Similarly the ϕ_{2s} orbitals in (2) and (3) and the ϕ_{2p} orbitals in (4) and (5) are also slightly different. In addition, in the HF approach we require that the $\phi_{1\bar{s}}$ and ϕ_{2s} orbitals in (2) and (3) be orthogonal.

The valence-bond (VB) wave functions for various low-lying excited states of He_2 would now be obtained by describing one He as in (1) and the other as in (2)–(5). However, there are some serious difficulties with the HF description of the atomic states. The HF energies of these states are compared with the experimental values[11] in Table I. Here we see that the HF energy for the ground state is too high by 1.1 eV, whereas the HF energies of the $2\,^3S$, $2\,^3P$, and $2\,^1P$ states are too high by 0.04, 0.11, and 0.03 eV, respectively. Such differences are expected. In the exact wave function the motions of the electrons are correlated so as to allow each electron to keep away from the other while remaining close to the nucleus. In the excited states one electron is in an excited orbital and on the average is far from the nucleus. Thus a (radial) correlation of the electrons is implicit in the HF wave function and hence the error is small. The HF description of the $1\,^1S$ state has both electrons in the same orbital and hence the correlation errors are large.

The $2\,^1S$ state, however, is different. Here the error is larger than for other $n=2$ states and it is *negative*, −0.64 eV. Thus the calculated energy is *lower* than the exact energy, implying that the HF wave function for this state has incorporated a significant piece of the ground-state wave function. We show below and in Appendix A that this results from the requirement that the $1\bar{s}$ and $2s$ orbitals be orthogonal to each other.

A generalization of the HF wave function, the generalized-valence-bond (GVB) wave function, ameliorates these problems. In this description there is a different orbital for every electron and each orbital is solved for variationally. Thus every singlet state is described as

$$(\phi_a\phi_b+\phi_b\phi_a)(\alpha\beta-\beta\alpha),$$

where ϕ_a and ϕ_b are different but *not* required to be orthogonal. In this case the ground-state wave function has the form

$$1\,^1S\text{:}\ (\phi_{1s}\phi_{1s'}+\phi_{1s'}\phi_{1s})(\alpha\beta-\beta\alpha), \tag{6}$$

and the $2\,^1S$ state becomes

$$2\,^1S\text{:}\ (\phi_{1\bar{s}}\phi_{2s}+\phi_{2s}\phi_{1\bar{s}})(\alpha\beta-\beta\alpha). \tag{7}$$

As shown in Figure 1 and Ref. 12a, orbitals ϕ_{1s} and $\phi_{1s'}$ are both similar to the HF $1s$ orbital except that one is closer to the nucleus and one is farther away. In this manner the GVB wave function incorporates essentially all of the radial correlation error. The self-consistent wave function (7) for the $2\,^1S$ state involves one orbital, $\phi_{1\bar{s}}$, that is similar to the ϕ_{1s} and $\phi_{1s'}$ orbitals[12b] of (6) (see Fig. 1).

By reexpressing (7) in terms of a configuration-interaction (CI) formulation,[13] one can show (see Appendix A) that the GVB energy is an upper bound on the exact energy for the $2\,^1S$ state. A similar approach applied to the HF wave function for the $2\,^1S$ state does not lead to an upper bound (see Appendix A).

In (7) the $1\bar{s}$ and $2s$ orbitals are not orthogonal. Modifying (7) by using $\phi_{2s'}=\phi_{2s}-\lambda\phi_{1\bar{s}}$ so that $\phi_{2s'}$ is orthogonal to $\phi_{1\bar{s}}$ (and taking $\phi_{1\bar{s}}$ to be approximately the same for HF and GVB), we obtain a three-term wave function

$$2\,^1S\text{:}\ (\phi_{1\bar{s}}\phi_{2s'}+\phi_{2s'}\phi_{1\bar{s}})+2\lambda\phi_{1\bar{s}}\phi_{1\bar{s}}. \tag{3'}$$

Thus as has been recognized before[14] the use of the orthogonality constraint is not consistent with the simple HF form (3) of the $2\,^1S$ wave function but is consistent with (3′). However substitution of the same transformation into the $2\,^3S$ wave function (2) does not change the wave function. In (4) and (5) the orbitals are already orthogonal by symmetry. Thus the states described in (2), (4), and (5) do

TABLE I. Energies[a] for the He atom (in eV).

State	HF Energy	HF Error[b]	GVB Energy	GVB Error[b]
$1\,^1S$	−77.870	1.135	−78.314	0.691
$2\,^3S$	−59.142	0.044	−59.142	0.044
$2\,^1S$	−59.025	−0.636	−58.327	0.062
$2\,^3P$	−57.932	0.109	−57.932	0.109
$2\,^1P$	−57.755	0.032	−57.755	0.032

[a]Energies are given in eV (1 eV = 0.036 749 a.u.). The calculated energies are obtained from a basis set consisting of six s-type, two p-type, and one d-type contracted Gaussians. For details, see Ref. 16.

[b]The energy error is given by (error) = (calculated energy) − (experimental energy). Experimental energies are from Ref. 11.

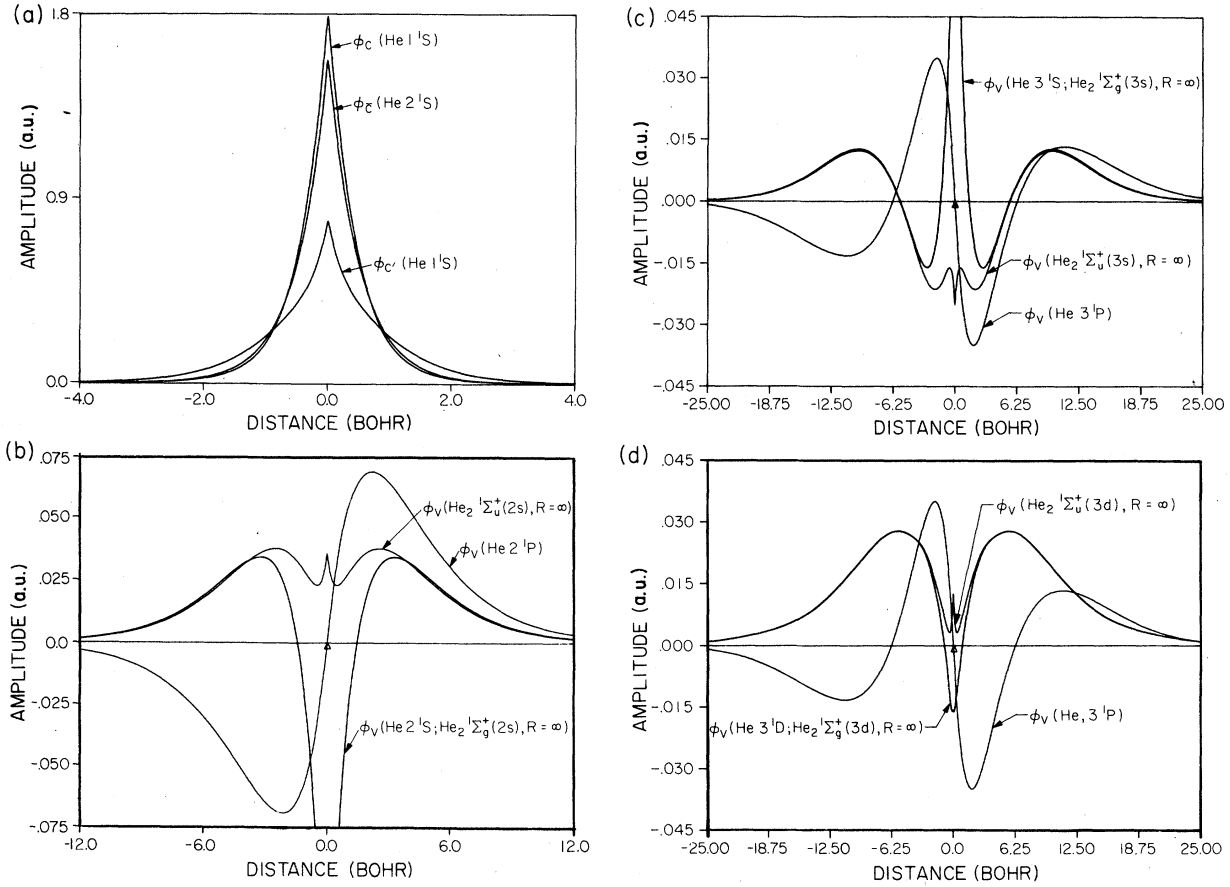

FIG. 1. (a) Core orbitals for the He atom. ϕ_c and $\phi_{c'}$ are from He 1^1S while $\phi_{\bar{c}}$ is the core orbital from He 2^1S. (b) $2s$ and $2p$ orbitals from atomic calculations (labelled with the atomic term symbols) and molecular calculations at $R=\infty$. See Refs. 16 and 18(d) for a discussion. (c) Same as (b) except $3s$ and $3p$ orbitals are shown. (d) Same as (b) except $3p$ and $3d$ orbitals are shown.

not change upon going from HF to GVB since taking the orbitals to be orthogonal in these states is not a restriction.

The GVB energies are listed in Table I, where we see that 39% of the error in the ground state has been removed and that the error in the $2\,^1S$ state is positive and small as for all other excited states. Thus the GVB wave function provides for a more consistent description of the states. However we can still visualize the total wave function in terms of electrons moving in various orbitals, each experiencing a (self-consistent) field due to the motions of other electrons. Proceeding beyond the GVB wave function to a CI-type wave function (incorporating additional correlation terms) or to the exact wave function leads to better energies but to a less interpretable wave function.

The orbitals for these GVB states are compared in Fig. 1. Although the (self-consistent GVB) $\phi_{1\bar{s}}$ orbital changes slightly from state to state, the changes are not of qualitative significance.

As a shorthand in describing the states of He we will use the symbols shown in Figs. 2(a)–(e) to describe the wave functions in (6), (2), (7), (4), and (5). Here two orbitals in the same row are understood to be singlet paired and two orbitals in the same column are understood to be triplet paired. As mentioned previously $\phi_{1\bar{s}}$ is different

	State	Symbol	Equation
(a)	$1\,^1S$ =	$\boxed{1s\ 1s'}$	(6)
(b)	$2\,^3S$ =	$\boxed{\begin{matrix}\overline{1s}\\ 2s\end{matrix}}$	(2)
(c)	$2\,^1S$ =	$\boxed{\overline{1s}\ 2s}$	(7)
(d)	$2\,^3P$ =	$\boxed{\begin{matrix}\overline{1s}\\ 2p\end{matrix}}$	(4)
(e)	$2\,^1P$ =	$\boxed{\overline{1s}\ 2p}$	(5)

FIG. 2. Wave function symbols for states of the He atom.

from state to state, ϕ_{2s} is different in Figs. 2(b) and 2(c), etc.

B. GVB wave functions for He_2

Although the HF wave function for the *ground state* of He_2 goes to the correct separated atoms limit as the molecule is pulled apart, the wave functions for the excited states do not dissociate correctly. In order to describe the correct molecular symmetry for the excited states of He_2, the HF orbitals must have the inversion symmetry of the molecule, i.e., g or u symmetry. This is not required in the spatially projected GVB wave function since the total wave function has the correct over-all symmetry even if the orbitals choose to be localized. As a result the GVB wave function dissociates correctly. We will see later that the flexibility of the GVB wave function in allowing for localized orbitals will be important in understanding some of the interactions determining the shapes of the potential curves. For these reasons and those discussed in Sec. II A, we use GVB wave functions to describe the excited states of He_2.

In order to construct the GVB wave functions of He_2 at $R=\infty$, we combine wave functions for the atoms as shown in Table II for the lower states. The short-hand shown in Fig. 3(a) indicates a singlet coupled pair

$$(\phi_{c_l}\phi_{c_l'}+\phi_{c_l'}\phi_{c_l})(\alpha\beta-\beta\alpha) \tag{8a}$$

on the left and a singlet coupled pair

$$(\phi_{\bar{c}_r}\phi_{v_r}+\phi_{v_r}\phi_{\bar{c}_r})(\alpha\beta-\beta\alpha)$$

on the right combined into a four-electron wave function corresponding to a singlet, i.e.,

$$\mathcal{A}[(\phi_{c_l}\phi_{c_l'}+\phi_{c_l'}\phi_{c_l})(\phi_{\bar{c}_r}\phi_{v_r}+\phi_{v_r}\phi_{\bar{c}_r})(\alpha\beta\alpha\beta)], \tag{8b}$$

where $\mathcal{A}$ is the four-electron antisymmetizer (de-

TABLE II. Frozen-orbital (FO) wave functions and tableau for some of the lower states of He_2.

Separated Atoms	Calculated Ionization Potential[a] at R = ∞	Molecular Symmetry[b]	Wavefunction at R = ∞[c]	Tableau at R = ∞[d]
$1^1S + 1^1S$	23.9	$X\,^1\Sigma_g^+$	$\psi_\ell(1^1S)\,\psi_r(1^1S)$	$\boxed{1s_\ell\ 1s_\ell'}$ / $\boxed{1s_r\ 1s_r'}$
$1^1S + 2^3S$	4.7	$c, a\,^3\Sigma_{g,u}^+(2s)$	$\psi_\ell(1^1S)\,\psi_r(2^3S) \pm \psi_\ell(2^3S)\,\psi_r(1^1S)$	$\boxed{1s_\ell\ 1s_\ell'}$ / $\boxed{1\bar{s}_r}$ / $\boxed{2s_r}$ $_{u,g}$
$1^1S + 2^1S$	3.9	$C, A\,^1\Sigma_{g,u}^+(2s)$	$\psi_\ell(1^1S)\,\psi_r(2^1S) \pm \psi_\ell(2^1S)\,\psi_r(1^1S)$	$\boxed{1s_\ell\ 1s_\ell'}$ / $\boxed{1\bar{s}_r\ 2s_r}$ $_{u,g}$
$1^1S + 2^3P$	3.5	$^3\Pi_{g,u}(2p)$	$\psi_\ell(1^1S)\,\psi_r(2^3P) \pm \psi_\ell(2^3P)\,\psi_r(1^1S)$	$\boxed{1s_\ell\ 1s_\ell'}$ / $\boxed{1\bar{s}_r}$ / $\boxed{2p_{\pi r}}$ $_{u,g}$
		$^3\Sigma_{g,u}(2p)$	$\psi_\ell(1^1S)\,\psi_r(2^3P) \pm \psi_\ell(2^3P)\,\psi_r(1^1S)$	$\boxed{1s_\ell\ 1s_\ell'}$ / $\boxed{1\bar{s}_r}$ / $\boxed{2p_{\sigma r}}$ $_{u,g}$
$1^1S + 2^1P$	3.3	$^1\Pi_{g,u}(2p)$	$\psi_\ell(1^1S)\,\psi_r(2^1P) \pm \psi_\ell(2^1P)\,\psi_r(1^1S)$	$\boxed{1s_\ell\ 1s_\ell'}$ / $\boxed{1\bar{s}_r\ 2p_{\pi,r}}$ $_{u,g}$
		$^1\Sigma_{g,u}(2p)$	$\psi_\ell(1^1S)\,\psi_r(2^1P) \pm \psi_\ell(2^1P)\,\psi_r(1^1S)$	$\boxed{1s_\ell\ 1s_\ell'}$ / $\boxed{1\bar{s}_r\ 2p_{\sigma,r}}$ $_{u,g}$

Note that the tableau $\boxed{1s_\ell\ 1s_\ell'}$ / $\boxed{1\bar{s}}$ / $\boxed{2s_r}$ $_g$ is shorthand for $\boxed{1s_\ell\ 1s_\ell'}$ / $\boxed{1\bar{s}_r}$ / $\boxed{2s_r}$ + $\boxed{1s_r\ 1s_r'}$ / $\boxed{1\bar{s}_\ell}$ / $\boxed{2s_\ell}$ and similarly $\boxed{1s_\ell\ 1s_\ell'}$ / $\boxed{1\bar{s}_r}$ / $\boxed{2s_r}$ $_u$ = $\boxed{1s_\ell\ 1s_\ell'}$ / $\boxed{1\bar{s}_r}$ / $\boxed{2s_r}$ - $\boxed{1s_r\ 1s_r'}$ / $\boxed{1\bar{s}_\ell}$ / $\boxed{2s_\ell}$

[a] Energies are in eV.

[b] This notation is used to describe all the molecular FO states. In $c, a\,^3\Sigma_{g,u}^+$ the c and a refer to the g and u subscripts, respectively.

[c] The upper and lower signs refer to the g and u states, respectively. We have omitted the antisymmetrizer, $\mathcal{A}$.

[d] We take the coordinate axes on the right He to be the inversion of those on the left He.

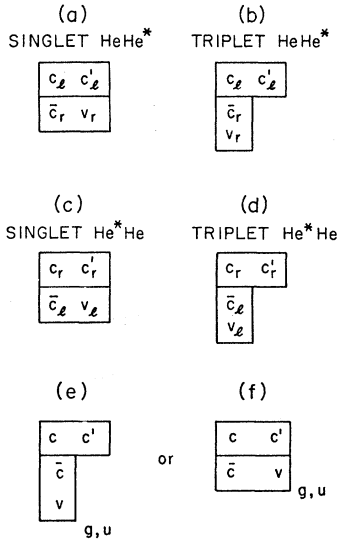

FIG. 3. Wave function symbols for the states of He_2^*.

terminant operator). Similarly, the shorthand shown in Fig. 3(b) indicates a singlet coupled pair [as in (8a)] on the left and a triplet coupled pair

$$(\phi_{\bar{c}_r}\phi_{v_r} - \phi_{v_r}\phi_{\bar{c}_r})(\alpha\beta + \beta\alpha)$$

on the right combined into a four-electron wave function corresponding to a triplet.

The wave functions in Figs. 3(a) and 3(b) describe

$$\psi_l(\mathrm{He})\psi_r(\mathrm{He}^*)$$

with the excitation on the right. However, excitation on the left leads to a wave function degenerate with the above. These two states interact, leading to optimum wave functions

$$\psi_l(\mathrm{He})\psi_r(\mathrm{He}^*) \pm \psi_r(\mathrm{He})\psi_l(\mathrm{He}^*) \qquad (8c)$$

of g and u inversion symmetry. Thus for the excited states of He_2 the wave functions are doubly degenerate at $R=\infty$. For large R ($R>7a_0$), the two states in (8c) are essentially degenerate, and we can understand the potential curves by examining either Fig. 3(a) for singlets or Fig. 3(b) for triplets. For small R the two states arising from (8c) have much different energies and it is necessary to add or to subtract the wave function of Fig. 3(c) from Fig. 3(a) in order to obtain a good description of the singlet states. Note that v_l is obtained by inverting v_r through the midpoint between the nuclei. (We refer to ψ_{3a} and $\psi_{3a} \pm \psi_{3c}$ as spatially unprojected and spatially projected wave functions, respectively.) $\psi_{3a} \pm \psi_{3c}$ then leads to both a $^1\Sigma_g^+$ state and a $^1\Sigma_u^+$ state as indicated in Table II. In a similar manner we obtain the four-electron triplet states.

Each of these states involves three similar $1s$-like core orbitals (ϕ_c, $\phi_{c'}$, and $\phi_{\bar{c}}$) and one Rydberg orbital (ϕ_v) that differ from state to state. Thus the wave functions we deal with all have the form shown in Fig. 3(e) or Fig. 3(f).

If the orbitals in Figs. 3(e) and 3(f) are solved for self-consistently at each internuclear distance, they are referred to as spatially projected GI [15,16] or generalized-valence-bond (GVB) orbitals for short.[17] This leads to different orbitals for the g and u states arising from the same separated-atoms limit (although for large R they are quite similar). If instead the orbitals are taken as the GVB orbitals of the atoms (at $R=\infty$) and are not allowed to adjust to the molecular potential, the over-all wave function is referred to as the frozen-orbital (FO) wave function. In this case the g and u states arising from the same separated-atoms limit use the same orbitals. Each of the orbitals have been expanded in terms of contracted Gaussian basis functions on each atom.[16] Thus when we refer to an orbital as being on the left or right He atom we really mean only that it is mostly on this center since all orbitals are expanded in a basis set that is equally partitioned between both centers (except of course for the FO wave functions).

III. FROZEN-ORBITAL (FO) POTENTIAL ENERGY CURVES

Figure 4 contains the FO potential curves obtained from the atomic wave functions shown in

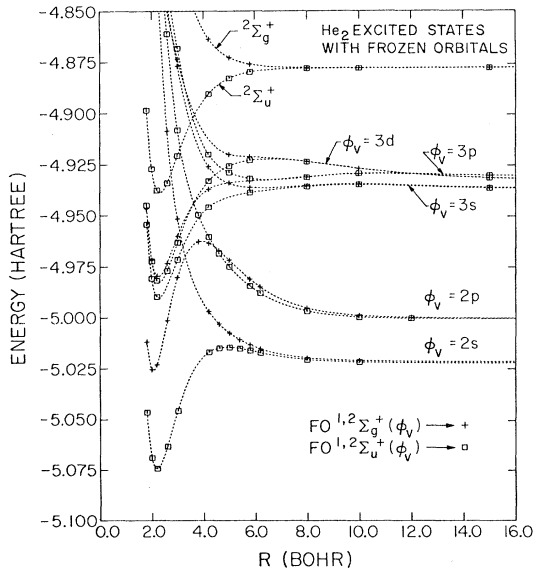

FIG. 4. Potential energy curves for the FO $^1\Sigma_g^+$ and $^1\Sigma_u^+$ excited states of He_2 and the $^2\Sigma_u^+$ and $^2\Sigma_g^+$ states of He_2^+. The FO wave functions from which these energies are calculated are composed of orbitals solved for self-consistently using projected wave functions at $R=\infty$.

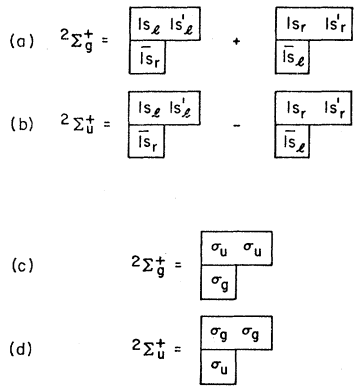

FIG. 5. Wave-function symbols for He_2^+.

Table II. We will denote the FO states as $^1\Sigma_g^+(n\,l)$ or $^1\Sigma_u^+(n\,l)$, where $n\,l$ denotes the atomic Rydberg orbital ϕ_v.

In order to understand the shapes of these curves, we must first consider the sizes of the Rydberg orbitals of atomic He. Amplitude plots of these orbitals are shown in Fig. 1. The values of $\langle z^2\rangle^{1/2}$ for these orbitals (in bohr) are as follows: 0.46 and 0.80 for $1s$ and $1s'$ (both from a GVB calculation on He $1\,^1S$), 3.30 for $2s$, 4.35 for $2p_z$, 7.70 for $3s$, 10.70 for $3p_z$, and 7.43 for $3d_{z^2}$. The equilibrium internuclear distance is about $2a_0$ for He_2^+ and for the bound excited states of He_2. Thus at R_e, the ϕ_v orbitals are all much larger than the molecule. Since most of the amplitude of these orbitals is not in the region between the two nuclei, it would appear that the binding is almost entirely due to the three core orbitals. The spatial extent of the Rydberg orbitals is further illustrated by the $R=\infty$ contour plots shown in Figs. 11 and 12. Thus near R_e the potential curves for the excited states of He_2 should resemble those of He_2^+.

For large R ($R>7a_0$) the two wave functions

$$\psi_l(\mathrm{He})\psi_r(\mathrm{He}^*) \quad \text{and} \quad \psi_r(\mathrm{He})\psi_l(\mathrm{He}^*)$$

are only weakly interacting, leading to two essentially degenerate states. We will now analyze the bonding for both small R and large R.

A. Small R

1. He_2^+ core-core interactions

Because of the important role expected to be played by interactions between the core orbitals at small R, we will first examine the core-core interactions with the Rydberg orbital deleted, i.e., we consider He_2^+.

Using the GVB atomic orbitals we obtain the two states shown in Figs. 5(a) and 5(b), i.e.,

$$\Phi_{g,u}=\mathcal{A}[(\phi_{1s_l}\phi_{1s_l'}\phi_{1\bar{s}_r}\pm\phi_{1s_r}\phi_{1s_r'}\phi_{1\bar{s}_l})(\alpha\beta-\beta\alpha)\alpha]\,.$$

If we take all the orbitals to be identical in shape ($\phi_{1s}=\phi_{1s'}=\phi_{1\bar{s}}$) but centered on the left and right nuclei, then the wave functions in Figs. 5(a) and 5(b) are equivalent to those in Figs. 5(c) and 5(d), respectively, where

$$\phi_{\sigma_g}=\phi_{1s_l}+\phi_{1s_r}$$

and

$$\phi_{\sigma_u}=\phi_{1s_l}-\phi_{1s_r}$$

(ignoring normalization). Since ϕ_{σ_g} is of bonding character while ϕ_{σ_u} is antibonding, we expect the $^2\Sigma_u^+$ state to be strongly bound while $^2\Sigma_g^+$ should be highly repulsive. Indeed this is the case, as shown in Fig. 4.

The VB-type description of He_2^+ is given in Figs. 5(a) and 5(b). In this case the splitting between $^2\Sigma_g^+$ and $^2\Sigma_u^+$ is usually referred to as resonance leading to the stabilization of $^2\Sigma_u^+$ and the destabilization of $^2\Sigma_g^+$.

2. He_2 core-core interactions

Consider the GVB wave function of an excited $^1\Sigma_u^+$ state of He_2 shown in Fig. 6(a). For an R *small* compared to the size of ϕ_v, we have

$$\phi_{v_r}\approx\phi_{v_l}\,,$$

i.e.,

$$\langle\phi_{v_r}|\phi_{v_l}\rangle\approx 1\,. \tag{9}$$

(For $\phi_{v_r}\approx-\phi_{v_l}$ see Ref. 18a and below.) For (9) the wave function in Fig. 6(a) becomes a product of that in Fig. 6(b) with ϕ_v (with this four-electron wave function then antisymmetrized).[18b] Thus Fig. 6(a) involves core interactions of the type in the $^2\Sigma_u^+$ state of He_2^+ and should lead to an attractive potential curve.

Starting with the positive $^1\Sigma_g^+$ superposition of states shown in Fig. 6(c) and applying (9), we find a core of the form shown in Fig. 6(d). Hence Fig. 6(c) should lead to a highly repulsive potential curve (since the core interactions are the same as in the $^2\Sigma_g^+$ state of He_2^+).

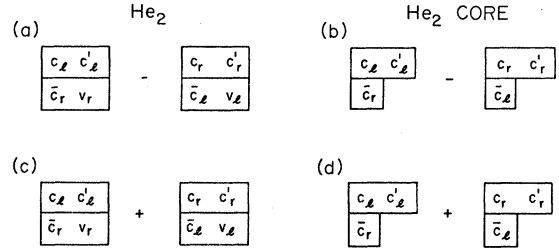

FIG. 6. Comparison of He_2 wave functions with the He_2^+ core part of this wave function (assuming $v_r\approx v_l$).

For the excited states with

$$\phi_v = 2s, 3s, 4s, 3d\sigma, 4d\sigma, \text{etc.}, \quad (10)$$

(9) applies and Fig. 6(a) leads to an attractive $^1\Sigma_u^+$ state while Fig. 6(c) leads to a repulsive $^1\Sigma_g^+$ state. For

$$\phi_v = 2p\sigma, 3p\sigma, 4f\sigma, \text{etc.}, \quad (11)$$

we have[18a] $\phi_{vr} \approx -\phi_{vl}$ and Fig. 6(a) leads to repulsive $^1\Sigma_u^+$ states in the manner of the $^2\Sigma_g^+$ state of He_2^+ while Fig. 6(c) leads to attractive $^1\Sigma_g^+$ states in the manner of the $^2\Sigma_u^+$ state of He_2^+. For

$$\phi_v = 2p\pi, 3p\pi, 4f\pi, \text{etc.}, \quad (12)$$

Fig. 6(a) leads to repulsive $^1\Pi_u$ states while the $^1\Pi_g$ states from Fig. 6(c) are attractive. For

$$\phi_v = 3d\pi, 4d\pi, \text{ etc.}, \quad (13)$$

Fig. 6(a) leads to attractive $^1\Pi_u$ states and Fig. 6(b) leads to repulsive $^1\Pi_g$ states. For $\phi_v = 3d\delta, 4d\delta$, etc., we have $\phi_{vl} \approx \phi_{vr}$ and hence the $^1\Delta_u$ states are attractive while the $^1\Delta_g$ states are repulsive. For $\phi_v = 4f\delta$, etc. we have $\phi_{vl} = -\phi_{vr}$ and hence the $^1\Delta_g$ states are attractive while the $^1\Delta_u$ states are repulsive. Similar considerations apply to the higher states. Since $\langle \phi_{vl} | \phi_{vr} \rangle$ depends upon R, the ratio of $^2\Sigma_g^+$ to $^2\Sigma_u^+$ core character in the four-electron wave function depends upon R.[16] The above conclusions apply equally well to the triplet states.[18c]

The above analysis partially explains the qualitative features of Fig. 4 (including which symmetries are bonding). If the valence orbitals were not further involved in determining the potential curves, then we would expect the potential curves of He_2 to have approximately the form indicated by the solid lines in Figs. 7(a) and 7(b). We see that this does indeed lead to a crude approximation to the FO potential curves but the differences are quite significant. Now we must examine the remaining effects.

B. Large R (Rydberg-core interactions)

At large R ($R > 7a_0$) the g and u states arising from each atomic level are essentially degenerate and hence we may understand the interactions at these distances by examining one component, such as Fig. 3(a), rather than Fig. 6(a) or Fig. 6(c). The wave function in Fig. 3(a) describes the interaction of a singlet pair localized on one atom with a singlet pair localized on another.

Because of the Pauli principle the wave function of the composite four-electron system cannot be taken as a product of the two-electron wave functions. Instead this product must be antisymmetrized. In effect this antisymmetrization places restrictions on the four-electron wave function, which in turn lead to an increase in the energy at

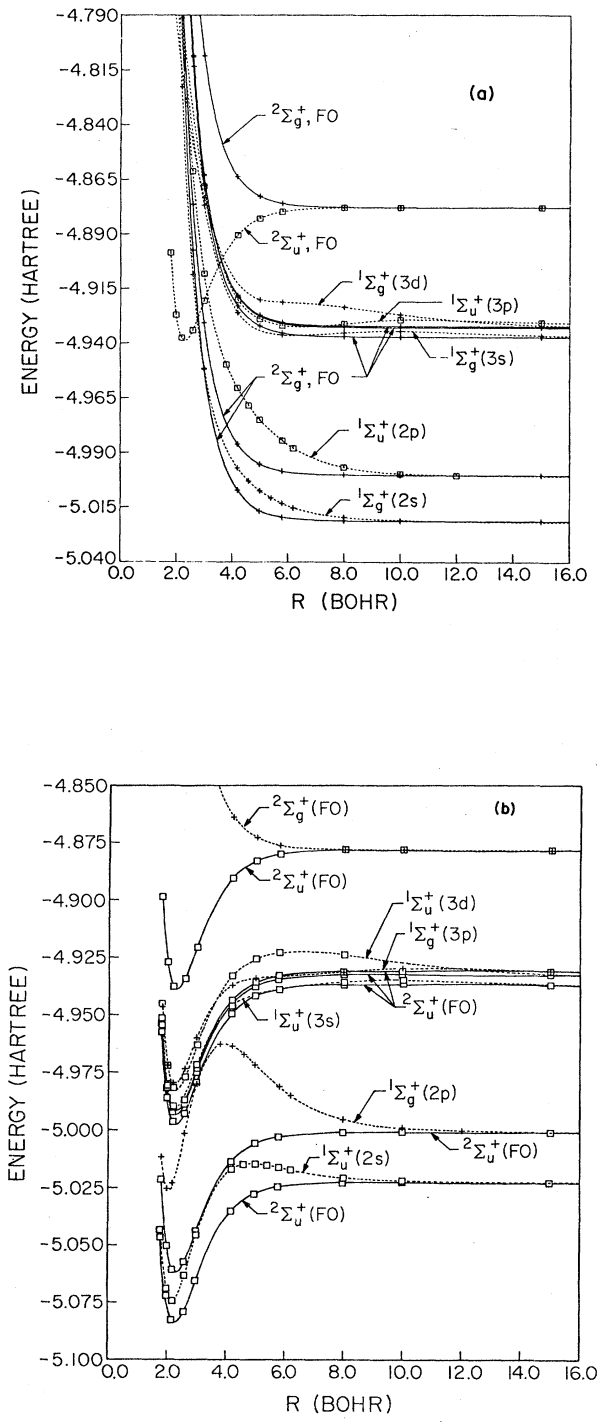

FIG. 7. (a) The totally repulsive FO energy curves for the excited states of He_2 shown with the attractive $^2\Sigma_u^+$ state and the repulsive (solid lines) $^2\Sigma_g^+$ state of He_2^+. The latter curve has been plotted to have the same asymptotic limit as the four-electron excited states. (b) Same as 7(a) except the attractive FO energy curves are shown with the $^2\Sigma_u^+$ state (solid lines), plotted to have the same asymptotic limit as the four electron states.

large R above that expected for a simple-product wave function. This energy increase is therefore a nonclassical effect and will be referred to as exchange or Pauli principle induced. This effect may be seen more clearly as follows. Since the orbitals on the left He in Fig. 3(a) are highly overlapping,[12b] we will take for the moment $\phi_{cl'} = \phi_{cl}$ as in the HF wave function. In this case the other orbitals, $\phi_{\bar{c}r}$ and ϕ_{vr}, of the antisymmetrized four-electron wave function can be orthogonalized to ϕ_{cl} without changing the total energy of the four-electron system. Thus we may replace $\phi_{\bar{c}r}$ and ϕ_{vr} by

$$\phi'_{\bar{c}r} = \phi_{\bar{c}r} - \lambda_1 \phi_{cl}\,, \qquad \phi'_{vr} = \phi_{vr} - \lambda_2 \phi_{cl} \tag{14}$$

(ignoring normalization). For large R the total energy is approximately the sum of the He ground-state energy and the He* energy *except* that the orthogonalized orbitals from (14) are used in the evaluating the energy of He*. Since the unorthogonalized orbitals $\phi_{\bar{c}r}$ and ϕ_{vr} were already optimum (at $R=\infty$), the orbitals in (14) should lead to a worse description of the right helium atom at large R. As a result for large R we expect the energy to increase as R is decreased. The mixing coefficients in (14) are

$$\lambda_1 = \langle \phi_{\bar{c}r} | \phi_{cl} \rangle$$

and

$$\lambda_2 = \langle \phi_{vr} | \phi_{cl} \rangle .$$

For large R we expect

$$\lambda_2 \gg \lambda_1$$

and hence the energy increase should depend primarily on λ_2. Since ϕ_{cl} is highly concentrated near the left nucleus as indicated in Fig. 1, we can view it as a δ function when compared to ϕ_v. Therefore we have

$$\lambda_2 \approx c\,\phi_{vr}(L)\,,$$

where $\phi_{vr}(L)$ is the amplitude of ϕ_{vr} evaluated at the left nucleus and is thus a function of R; c is a constant approximately independent of R.

By an independent approach (discussed elsewhere[16]) based on a study of a partition of the total energy at various R and an analysis of the exchange kinetic energy, we find the total energy to vary approximately as λ_2^2. As a result the potential curve is shaped at large R as the square of the amplitude of the Rydberg orbital on the opposite center. Thus we can now understand the shapes of the FO curves in Fig. 4 from the orbital amplitude plots of Fig. 1. For example, the $\phi_v = 2s$ orbital increases in amplitude as r (distance from its center) decreases from ∞ to about $3.3a_0$.[18d] Thus we find the potential curves in Fig. 4 arising from $\phi_v = 2s$ to rise as R is decreased, following the square of the amplitude of the Rydberg orbital. This continues until about $6.5a_0$ where the core-core interactions begin to become important. (The $^2\Sigma_u^+$ and $^2\Sigma_g^+$ curves for He_2^+ become noticeably split at this distance.) For smaller R we must consider wave functions [Fig. 6(a)] and [Fig. 6(c)] rather than just Fig. 3(a). As a result, the $^1\Sigma_u^+(2s)$ curve reaches a maximum, and due to favorable core-core interactions falls to an attractive minimum. The $^1\Sigma_g^+(2s)$ curve has unfavorable core-core interactions and becomes totally repulsive, crossing higher FO curves.

For the FO curves with $\phi_v = 2p$ the splitting of the u and g states occurs at smaller R (near $4a_0$) than for $^1\Sigma_{u,g}^+(2s)$. In order to understand this we recall that because $\phi_{vr} \approx -\phi_{vl}$ at small R the core-core interactions split the u and g potential curves arising from the same separated-atoms limit. For $\phi_v = 2p$ we note that instead of monotonically approaching -1 as R decreases, $\langle \phi_{vr} | \phi_{vl} \rangle$ is positive at large R (since a lobe of the right p orbital overlaps the lobe of the same sign of the left one). This overlap first increases and then decreases as R decreases, vanishes near $5a_0$, and becomes more negative as R decreases further. Thus due to the Rydberg-Rydberg overlap the core-core splitting does not dominate until R is decreased to $4a_0$ as compared to $R = 6.5a_0$ for the curves arising from $\phi_v = 2s$. In order to understand the region $4a_0 < R < 7a_0$, we must also consider the Rydberg-core interactions. Along its axis the $2p$ orbital has greater amplitude than the $2s$ orbital for $r > 2.2a_0$ (see Fig. 1). Thus the repulsive Rydberg-core interactions discussed above are larger for $\phi_v = 2p$ and we expect a larger hump in the attractive $^1\Sigma_g^+(2p)$ curve than for the attractive $^1\Sigma_u^+(2s)$ curve. This difference is further enhanced by the presence of a favorable core-core interaction, which overwhelms the unfavorable Rydberg-core interaction near $R = 6a_0$ for $^1\Sigma_u^+(2s)$ but does not do the same until about $R = 4a_0$ for $^1\Sigma_g^+(2p)$. This also causes the $^1\Sigma_g^+(2p)$ state to have its hump at smaller R than that for the $^1\Sigma_g^+(2s)$ state.

The $\phi_v = 3s$ and $3p$ orbitals each have a maximum at large R (see Fig. 1 and below), but the amplitude at this maximum is much smaller than the maximum amplitudes found for the $2s$ and $2p$ orbitals. Thus we find a small maximum at large R in the potential curves. For smaller R the energies decrease as the amplitudes of the $\phi_v = 3s$ and $3p$ orbitals decrease with decreasing r. Since these orbitals have nodes at $5.5a_0$ and $6.3a_0$, respectively (i.e., $\lambda_2 = 0$), the potential curves return to the $R = \infty$ energy before being split by the core-core interactions. For $\phi_v = 3s$ and $3p$, the

maximum in the orbital amplitudes occurs at $9.8a_0$ and $11.0a_0$, respectively, while the maximum in the potential curves comes at $9.8a_0$ and $10.5a_0$, respectively.

Figure 1 shows that the amplitude of $\phi_v = 3d$ has a maximum near $5.7a_0$ and crosses the amplitude of $\phi_v = 3p$ near $12.5a_0$. As a result the $^1\Sigma^+_{u,g}(3d)$ potential curves cross those of $^1\Sigma^+_{u,g}(3p)$ and become increasingly repulsive as R decreases toward $6a_0$. At this distance the core-core interactions intercede leading to separation of the $^1\Sigma^+_g$ and $^1\Sigma^+_u$ curves with $^1\Sigma^+_u$ lower (as expected).

Thus the Pauli principle should lead to repulsive character at large R in all $^1\Sigma$ states just as is observed in Fig. 2. The same effect operates also for $^3\Sigma$ states. For $^{3,1}\Pi$, $^{3,1}\Delta$ states, etc., $\lambda_2 = 0$ and hence we do not expect a maximum at large R.

IV. SCF-GVB POTENTIAL CURVES

Below we show that the shapes of the resulting SCF-GVB potential curves for the various states can be understood quite easily in terms of the FO description discussed above.

We denote the SCF-GVB curves by the term symbol followed by parentheses enclosing the character of the Rydberg orbital at R_e (e.g., $2s\sigma, 2p\sigma$, etc.) followed by the character of the same orbital at $R = \infty$. Thus $^1\Sigma^+_g(2p\sigma, 2s)$ indicates the state that has $2s$ character at $R = \infty$ and $2p\sigma$ character at R_e.

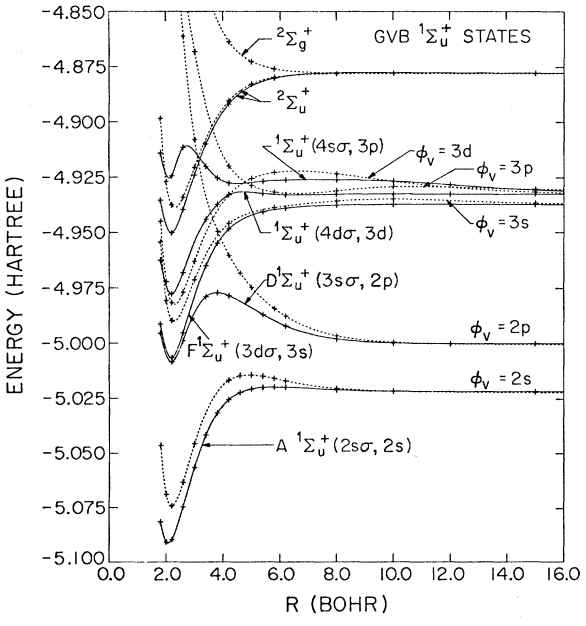

FIG. 8. FO (dashed) and SCF-GVB (solid) energy curves for the excited $^1\Sigma^+_u$ states of He_2. Also shown is an FO curve for $^2\Sigma^+_g$, He_2^+, and FO and SCF-GVB curves for $^2\Sigma^+_u$, He_2^+.

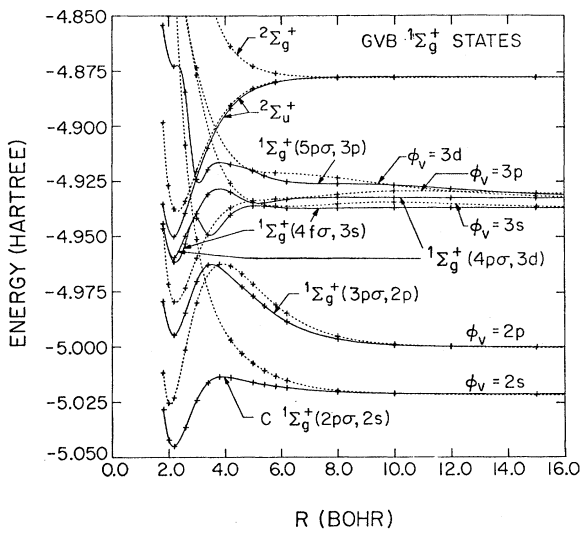

FIG. 9. FO (dashed) and SCF-GVB (solid) energy curves for the excited $^1\Sigma^+_g$ states of He_2. Also shown is an FO curve for $^2\Sigma^+_g$, He_2^+, and FO and SCF-GVB curves for $^2\Sigma^+_u$, He_2^+.

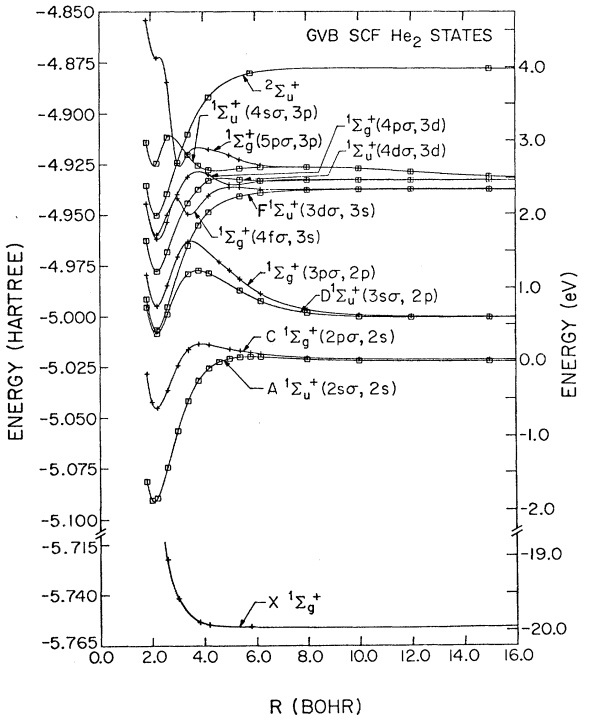

FIG. 10. SCF-GVB energy curves for the excited $^1\Sigma^+_g$ and $^1\Sigma^+_u$ states of He_2. Also shown are SCF-GVB curves for $X\ ^1\Sigma^+_g$ and $X\ ^2\Sigma^+_u$ of He_2^+.

The SCF-GVB curves are shown as the solid lines in Figures 8, 9, and 10. Contour plots of the SCF-GVB Rydberg orbitals are shown in Figs. 11 and 12.

A. The $A\,^1\Sigma_u^+(2s\sigma,2s)$ state

The A state has been the most widely discussed excited state of He_2.[18e] Although it is the second excited state (lying above $a\,^3\Sigma_u^+$), it is the lowest state to be dipole connected to the repulsive ground state. It is also the upper state for the transitions giving rise to the continuum vacuum uv (~600–1100 Å) emissions mentioned above.

Nevertheless, the shape of the A-state potential curve has not been well understood. In the past, humps in potential curves (for nonrotating molecules) have generally[19] (with the exception of Ref. 20) been attributed to an avoided crossing of a lower repulsive curve with a higher attractive curve of the same symmetry (leading to a lower adiabatic curve containing a hump). It is easily seen that this cannot explain the hump in the A state since the FO curve for this state has a hump and does not cross any other curves. Thus the hump in the FO potential curve arises from a new effect: the Pauli-principle-induced Rydberg-core repulsive interaction combined with an attractive core-core interaction as discussed in Sec. III.

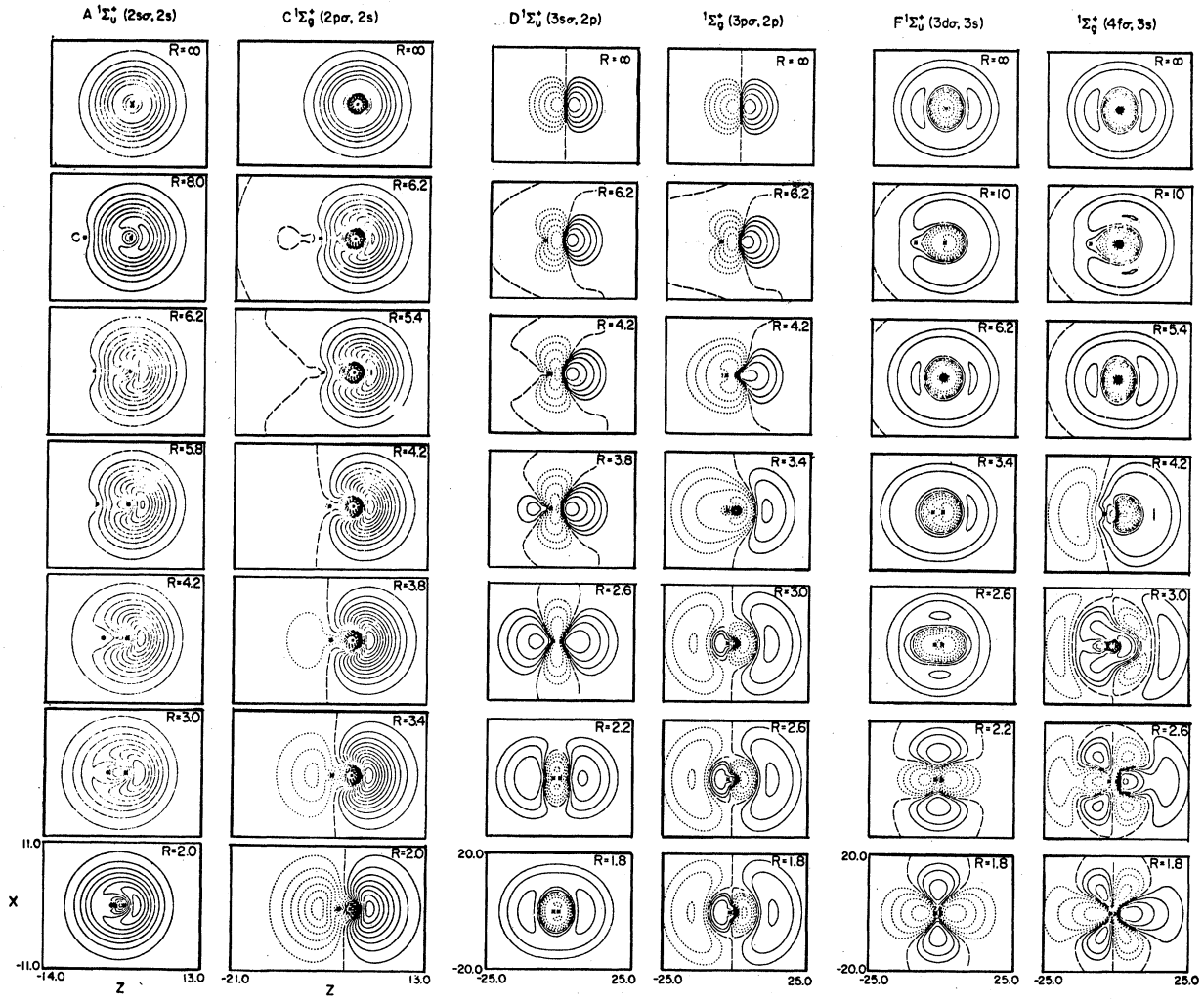

FIG. 11. Contour plots of the GVB Rydberg orbitals are shown at several internuclear distances for several states. The contours are plotted in a plane containing the internuclear axis with the two centers shown by small asterisks. The contour with long dashes indicates the nodal plane. The positive contours are solid lines while the negative contours are dotted. For the A and C states the contour interval is 0.005 and contours more negative than −0.050 are not shown. For the other states the contours plotted are of absolute value 0.0025, 0.0050, 0.0100, 0.0200, and 0.0400. Distances are in bohr.

The SCF-GVB potential curve shown in Fig. 8 is quite similar to the FO potential curve with the maximum coming at nearly the same location. From Fig. 11 we see that except for a slight polarization away from the opposite center, the Rydberg orbital does not change shape appreciably as R is decreased from ∞ to R_e. Therefore the hump in the SCF-GVB potential curve arises from the same interactions as found in the FO potential curve. Since the shape of the SCF-GVB potential curve in the region of the hump agrees well with experimental results (see Sec. V), we conclude that the above described Pauli-principle–induced repulsive interaction is responsible for the maximum observed in the $A\,^1\Sigma_u^+$ and therefore also in the $a\,^3\Sigma_u^+$ state.

B. The $C\,^1\Sigma_g^+(2p\sigma, 2s)$ state

The $^1\Sigma_g^+(2s)$ FO state is totally repulsive due to the unfavorable Rydberg-core interaction at large R (as in $A\,^1\Sigma_u^+$) and the repulsive core-core interaction at small R. From Fig. 4 we see that this repulsive curve crosses the attractive part of $^1\Sigma_g^+(2p)$ (having a favorable core-core interaction). Thus we would expect the SCF-GVB curve to be similar to $^1\Sigma_g^+(2s)$ at large R and to $^1\Sigma_g^+(2p)$ at small R. As can be seen in Fig. 9, this leads to an avoided curve crossing and therefore a maximum in the $C\,^1\Sigma_g^+(2p\sigma, 2s)$ potential curve. In addition we expect the Rydberg orbital to reflect the avoided crossing and to change from $2s\sigma$-like at large R to $2p\sigma$-like at small R. This is shown in Fig. 11. Because of the avoided crossing, the $C\,^1\Sigma_g^+(2p\sigma, 2s)$ state has a shallow well compared to the A state (see Fig. 10 and Table III). Upon subtracting the energy of the C state at R_e from the energy at the maximum in $^1\Sigma_g^+(2p)$ we obtain 1.85 eV, in good agreement with the binding energy of 1.88 eV (or 1.94 eV if we take the binding energy to be the difference between the maximum and minimum energies) found for the $A\,^1\Sigma_u^+$ state.

Mulliken[19] has offered an explanation for the origin of the large maximum in the C state and for those found in other He_2 potential curves. In his description, states will have large "obligatory" humps when the principal quantum number of the Rydberg orbital at the united-atom limit is greater than the corresponding quantum number at the separated-atom limit. He assumed that the united-atom limit of the Rydberg orbital is important near R_e. For cases in which the united-atom Rydberg orbital is unpromoted (e.g., $A\,^1\Sigma_u^+$) he expected no large humps. Humps in such potential curves were classified as "nonobligatory" or unexplained. For the C state, Mulliken took the united-atom limit of the Rydberg orbital (based on the H_2^+ correlation diagram) to be $3p\sigma$ and thus expected a large hump since $\phi_v = 2s$ at $R = \infty$. However, we find that the repulsive part of the potential curve arises from the unfavorable Rydberg-core interactions and are indeed present in the FO curve with $\phi_v = 2s$ at all R (no promotion). We find that the Rydberg orbital for the C state becomes $2p\sigma$-like near R_e (rather than $3p\sigma$-like), leading to strong bonding character in the potential curve. The valence orbital remains $2p\sigma$-like (although diffuse) and unpromoted into our smallest separation of 1.8 bohr. This is further supported by the fact that calculations[16] on the ground state show that the core orbitals remain localized and $1s$-like into $R = 1.8a_0$ and do not choose to resemble a $2p\sigma$-like symmetry function. As a result the $2p\sigma$ character is found in the first excited $^1\Sigma_g^+$ state while $3p\sigma$ is found in the third $^1\Sigma_g^+$ state at $R = 1.8a_0$.

C. The $^1\Sigma_g^+(3p\sigma, 2p)$ state

Figure 9 shows that for $R > 4a_0$ the FO and SCF $^1\Sigma_g^+$ curves arising from the $2p$ separated-atom limit are quite similar. Indeed Fig. 11 shows that for $R > 4.2a_0$ the Rydberg orbital remains mostly $2p\sigma$-like. Thus, in this region, we consider the interactions giving rise to the shape of the SCF curve to be the same as those which determine the FO curve. (Here again no promotion effect[19] is involved in the repulsive character at large R.)

Nevertheless, as R is decreased further toward R_e, the Rydberg orbital cannot remain $2p\sigma$-like since this character is present in the lower $C\,^1\Sigma_g^+(2p\sigma, 2s)$ state. As a result $^1\Sigma_g^+(3p\sigma, 2p)$ obtains $3p\sigma$ character from the next FO curve of g symmetry having an attractive core-core interaction (see Fig. 9). This is clearly shown in Fig. 11, where for $R < 4.2$ bohr the Rydberg orbital loses its $2p\sigma$ character and becomes $3p\sigma$-like. (This could be considered a promotional effect of the type attributed by Mulliken to the lower C state. But note that the "promotion" causes the potential curve to fall and not to rise.) The minimum in the $^1\Sigma_g^+(3p)$ FO curve lies above the separated-atoms energy for $^1\Sigma_g^+(2p)$. While SCF adjustment accounts for some lowering, the minimum of $^1\Sigma_g^+(3p\sigma, 2p)$ remains slightly above its separated-atom limit.

D. The $D\,^1\Sigma_u^+(3s\sigma, 2p)$ state

Because of unfavorable Rydberg-core interactions, the SCF-GVB curve and the FO-GVB curves are repulsive at large R (see Fig. 8). For $R < 4a_0$ the FO curve continues to rise because of an unfavorable core-core interaction, crossing the other attractive FO curves (possessing a favorable core-core interaction), $^1\Sigma_u^+(3s)$ and $^1\Sigma_u^+(3d)$. This leads to an avoided crossing and a maximum in the SCF-GVB curve. Figure 11 shows that the Ryd-

TABLE III. Extrema in the He_2 potential curves.[a]

	R_e (Å)	D_e (eV)	R_{max} (Å)	ΔE_{max}[b] (eV)
$A\,^1\Sigma_u^+(2s\sigma, 2s)$				
This work	1.10	1.883	3.08–3.09[c]	0.0607
Previous *ab initio*,				
Ref. 2(d)	1.082	2.469 ± 0.006	•••	•••
Ref. 20	•••	•••	3	0.084
Ref. d	1.040	2.306	2.8	0.086
Ref. e	1.12	1.719	2.76	0.153
Experimentally derived,				
Ref. 2(a)	1.04	2.5	3.1	0.05
Ref. 21(b)	•••	•••	3.1	0.049 ± 0.010
Ref. 2(c)	•••	2.55 ± 0.17	3.0 ± 0.3	0.03 ± 0.03
Ref. 2(b)	•••	2.50 ± 0.03	•••	•••
Ref. 23	1.039	•••	•••	•••
Ref. 3	•••	•••	•••	.059
$C\,^1\Sigma_g^+(2p\sigma, 2s)$				
This work	1.15	0.6443	2.06	0.216
Previous *ab initio*,				
Ref. 24	•••	•••	2.4	0.7
Ref. f	1.14	0.89	•••	•••
Experimentally derived,				
Ref. 23	1.091	•••	•••	•••
$D\,^1\Sigma_u^+(3s\sigma, 2p)$				
This work	1.15	0.221	1.99	0.6288
Experimentally derived,				
Ref. 27	1.069			
$^1\Sigma_g^+(3p\sigma, 2p)$				
This work	1.16	−0.153	1.86	1.025
$F\,^1\Sigma_u^+(3d\sigma, 3s)$				
This work	1.16	1.881	6.02–6.11[c]	0.0040
Experimentally derived,				
Ref. 28	1.089	•••	•••	•••
Ref. 3	•••	•••	•••	0.0074
$^1\Sigma_g^+(4f\sigma, 3s)$				
This work	1.19	0.6694	1.57	−0.120
	1.84[g]	0.3390[h]	2.72	0.0296
	3.62–3.70[c,g]	0.0057[h]	6.09–6.10[c]	0.0040
$^1\Sigma_u^+(4d\sigma, 3d)$				
This work	1.16	1.220	2.48–2.49[c]	0.0323
	3.42[g]	0.0059[h]	5.12–5.29[c]	0.0062
$^1\Sigma_g^+(4p\sigma, 3d)$				
This work	1.15	0.7303	2.02	0.119
	2.75[g]	0.0571[h]	4.32–4.36[c]	0.011

[a] All energies are in eV (1 eV = 0.036 749 a.u.) and distances are in Å (1 Å = $1.890a_0$). The results of this work have been obtained from a cubic spline fit of the calculated energies (see Ref. 16) and are shown in the first row for each state.

[b] $\Delta E_{max} = E(R = R_{max}) - E(R = \infty)$.

[c] To the accuracy reported the potential curve has a vanishing slope in this region.

[d] S. Mukamel and U. Kaldor, Mol. Phys. 22, 1107 (1971).

[e] D. R. Scott, E. M. Greenawalt, J. C. Browne, and F. A. Matsen, J. Chem. Phys. 44, 2981 (1966).

[f] E. M. Greenawalt (unpublished) [see F. A. Matsen, *Advances in Chemical Physics* (Wiley-Interscience, New York, 1971), Vol. XXI, p. 1.]

[g] This is a local minimum and is not R_e.

[h] This is a local minimum and is not D_e.

berg orbital remains $2p\sigma$-like for $R > 4.2a_0$. As R is decreased the orbital first becomes $3d\sigma$-like before becoming $3s\sigma$-like for $R < 2.2a_0$. The overlap and Hamiltonian matrix elements at $3.8a_0$ are about a factor of 30 greater for interaction between the $^1\Sigma_u^+(2p)$ and $^1\Sigma_u^+(3d)$ states as compared to $^1\Sigma_u^+(2p)$ and $^1\Sigma_u^+(3s)$. (For a detailed discussion of this interaction see Ref. 16a.)

Near $R = 2.2a_0$ the SCF-GVB $D^1\Sigma_u^+(3s\sigma, 2p)$ and $F^1\Sigma_u^+(3d\sigma, 3s)$ states become nearly degenerate, and indeed they switch character (see Fig. 11) between $2.2a_0$ and $2.0a_0$ (see Sec. V for a further discussion of this near degeneracy).

Although Mulliken[19] describes this state as being $3d\sigma$-like near R_e, we see that a promotional effect is not responsible for the repulsive character at $R > 4a_0$. Incorporation of $3d\sigma$ character was necessary though in order that the curve have an attractive well.

E. The $F^1\Sigma_u^+(3d\sigma, 3s)$ and $^1\Sigma_g^+(4f\sigma, 3s)$ states

From Figs. 8 and 11[21a] we see that the $^1\Sigma_u^+ \times (3d\sigma, 3s)$ state is analogous to the A state, with the FO wave function providing a good qualitative description. In the SCF wave function the Rydberg orbital remains $3s\sigma$-like until about 2.2 bohr. Thus the potential curve is quite similar in shape to the A state, having virtually the same dissociation energy (see Table III). For $R \sim 2a_0$ the $D^1\Sigma_u^+ \times (3s\sigma, 2p)$ and $F^1\Sigma_u^+(3d\sigma, 3s)$ states are nearly degenerate, and the calculated wave functions exchange character, as mentioned above.

At large R both the $F^1\Sigma_u^+(3d\sigma, 3s)$ and $^1\Sigma_g^+(4f\sigma, 3s)$ states are nearly degenerate and there is little qualitative difference between the FO-GVB and SCF-GVB descriptions of these states. The unfavorable Rydberg-core interactions lead to a small maximum in the SCF-GVB potential curves near $11.5a_0$, resulting from the overlap of the outer maximum of the $3s\sigma$ Rydberg orbital with the core orbitals on the opposite center. The potential curves fall as R decreases from the distance corresponding to the outer maximum in the Rydberg orbital.

For $^1\Sigma_g^+(4f\sigma, 3s)$ the repulsive-core FO curve $^1\Sigma_g^+(3s)$ rises and crosses the attractive curve resulting from $^1\Sigma_g^+(3p)$ near $5a_0$ (see Fig. 9). This results in an avoided crossing of the SCF curves, causing a maximum for $^1\Sigma_g^+(4f\sigma, 3s)$ and a small dip for $^1\Sigma_g^+(4p\sigma, 3d)$. Figure 11[21a] shows $3p\sigma$ character mixing into $^1\Sigma_g^+(4f\sigma, 3s)$ at $R = 4.2a_0$. For smaller R there is apparently a strong interaction with the repulsive-core FO state arising from $\phi_v = 2s$ leading to another maximum in the curve near $R = 3a_0$. In order for $^1\Sigma_g^+(4f\sigma, 3s)$ to be attractive near R_e, it must have an avoided crossing with a higher ($n = 4$) state in order to obtain attractive $^2\Sigma_u^+$ core. (There are no remaining favorable $n = 3$ FO curves.) Both the $^1\Sigma_g^+(4f)$ and $^1\Sigma_g^+(4p)$ states can contribute since they provide attractive core interactions. These states[11] are separated by only 39 cm^{-1} at $R = \infty$ with $^1\Sigma_g^+(4f)$ being lower. $^1\Sigma_g^+(5f)$ and $^1\Sigma_g^+(5p)$ are about 2200 cm^{-1} above these states and may also be important (although our basis set[16] will not provide a good description of these orbitals). From Figure 11 we see that $^1\Sigma_g^+(4f\sigma, 3s)$ becomes $4f\sigma$-like near R_e. Our basis set[16] does not contain any $4f$ basis functions and indeed the $4f$ orbital shown in Fig. 11 is somewhat tighter than a hydrogenic $4f$. The inclusion of $n = 4$ basis functions could substantially improve the quantitative description of the potential curves in this region.

F. The $^1\Sigma_g^+(4p\sigma, 3d)$ and $^1\Sigma_u^+(4d\sigma, 3d)$ states

In the discussion of the FO curves we noted that because of the shapes of the $\phi_v = 3d$ and $\phi_v = 3p$ orbitals, the energy curves cross near $R = 12a_0$. We expect this to lead to an avoided crossing of the SCF curves, and this is shown in the contour plots of Fig. 12. Here we see that the Rydberg orbitals of the $^1\Sigma_u^+(4d\sigma, 3d)$ and $^1\Sigma_g^+(4p\sigma, 3d)$ states become $3p\sigma$-like while those for the $^1\Sigma_u^+(4s\sigma, 3p)$ and $^1\Sigma_g^+(5p\sigma, 3p)$ states become $3d\sigma$-like as R is decreased to $6.2a_0$.

The maximum in the potential curve for $^1\Sigma_g^+(4p\sigma, 3d)$ does not come until $R = 8.2a_0$ (see Table III) and can be explained by the near degeneracy of the $^1\Sigma_g^+(4p\sigma, 3d)$ and $^1\Sigma_g^+(5p\sigma, 3p)$ states at $R = \infty$. The orbitals of these states (and the corresponding u states) at very large R ($R > 15a_0$) are represented by approximately orthogonal linear combinations of $3d\sigma$ and $3p\sigma$ character. The orbital for the lowest energy combination is shown at $R = 15a_0$ in the first two columns of Fig. 12.[21a] This orbital is significantly polarized away from the opposite He and causes the maximum in the SCF curve to come at much smaller R than that which would be expected from the crossing of the FO curves. For the higher $^1\Sigma_g^+(5p\sigma, 3p)$ and $^1\Sigma_u^+(4s\sigma, 3p)$ states the orbital is similar except that it is polarized toward the opposite He (see the last two columns of Fig. 12) resulting in more repulsive energy curves in this region. Note that a similar mixing effect occurs to a much smaller degree at large R for the $^1\Sigma_g^+(2p\sigma, 2s)$ and $^1\Sigma_g^+(3p\sigma, 2p)$ states (and the corresponding u states) because of their large energy separation. $3p\sigma$ becomes dominant in the Rydberg orbital of $^1\Sigma_g^+(4p\sigma, 3d)$ near $R = 10a_0$ and remains as R is decreased to $5.4a_0$. Note that the $^1\Sigma_g^+(3p)$ and $^1\Sigma_g^+(4p\sigma, 3d)$ states are nearly degenerate near $R = 7a_0$ (see Fig. 9). The small well in $^1\Sigma_g^+(4p\sigma, 3d)$

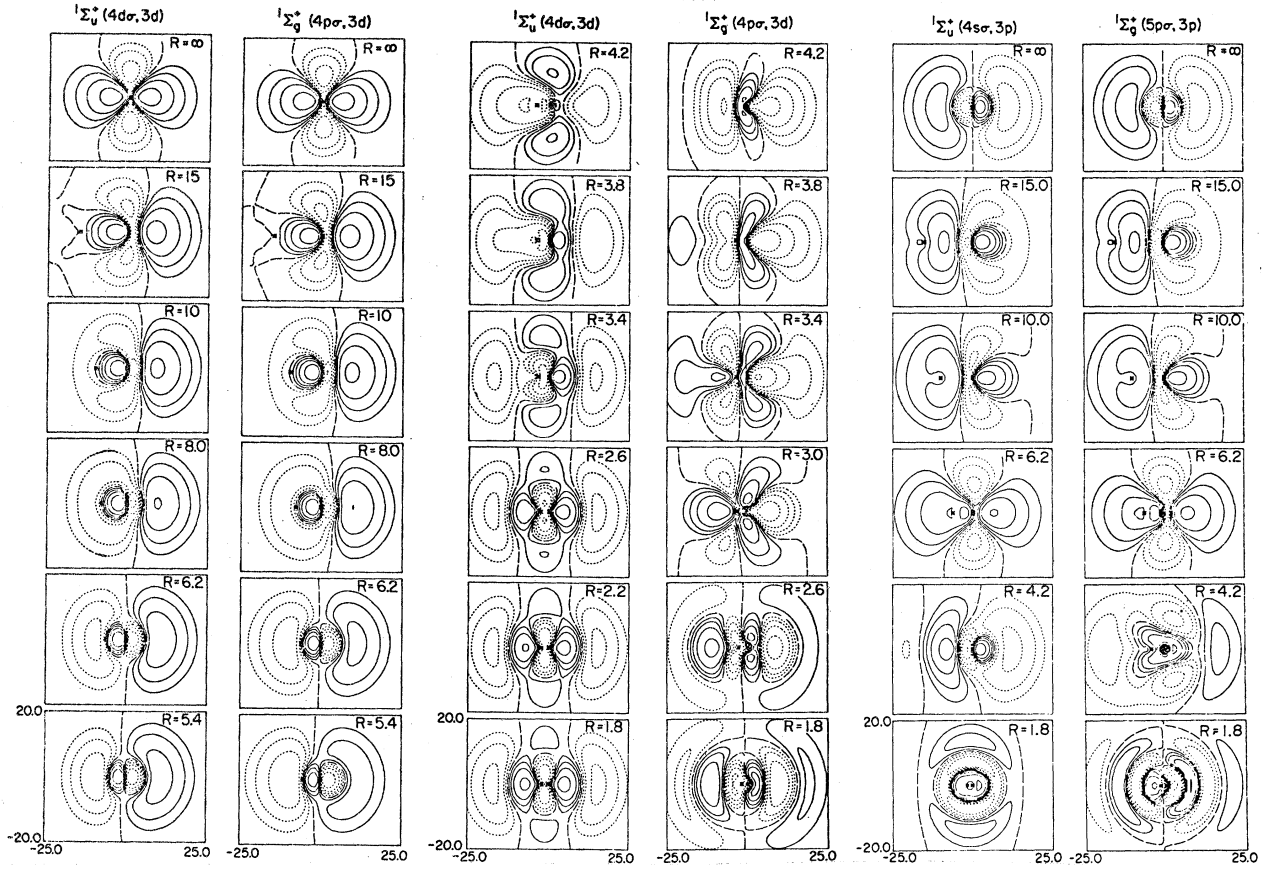

FIG. 12. Contour plots of the GVB Rydberg orbitals are shown at several internuclear distances for several states. The conventions are the same as for Fig. 11.

(see Table III) at $R=5.2a_0$ has been discussed in Sec. IV E and is due to $3s\sigma$ character shown mixing in at $R=4.2a_0$ in Fig. 12. Because the Rydberg orbital is now g-like necessitating unfavorable $^2\Sigma_g^+$ core character, the potential curve rises. In order to fall to a minimum at R_e, it must mix in favorable core character from a FO state arising from an $n=4$ atomic state. We see from Fig. 12 that $4f\sigma$ character mixes into the Rydberg orbital between $R=3.8a_0$ and $3.0a_0$, causing the potential curve to fall from a maximum at $3.8a_0$. At $R=3.0a_0$ $^1\Sigma_g^+(4p\sigma, 3d)$ becomes nearly degenerate with the rising $^1\Sigma_g^+(4f\sigma, 3s)$ state. The $4f\sigma$ character is transferred to the Rydberg orbital of the latter state which then becomes attractive while the Rydberg orbital for $^1\Sigma_g^+(4p\sigma, 3d)$ mixes in favorable $4p\sigma$ character causing the potential curve to fall to a minimum at $R=2.17a_0$. Once again the inclusion of $n=4$ basis functions in this region would substantially improve our quantitative description.

For $^1\Sigma_u^+(4d\sigma, 3d)$ and $R<6.2a_0$, the SCF curve follows the repulsive $^1\Sigma_u^+(3p)$ curve. Near $R=5a_0$ the latter curve has a second crossing with $^1\Sigma_u^+(3d)$. The mixing in of $3d\sigma$ character is shown at $R=4.2a_0$ and $3.8a_0$ of Fig. 12.[21a] At $R=3.8a_0$, $3d\sigma$ character is important in $^1\Sigma_u^+(3s\sigma, 2p)$ and as a result $^1\Sigma_u^+(4d\sigma, 3d)$ must mix with states having $n=4$ Ry orbitals in order to have an attractive potential well near R_e. Figure 12 shows that near $R=3.4a_0$, $4d\sigma$ character becomes important and remains as R decreases to R_e.

G. The $^1\Sigma_g^+(5p\sigma,3p)$ and $^1\Sigma_u^+(4s\sigma,3p)$ states

The polarization of the Rydberg orbitals near $R=15.0a_0$ has been discussed in Sec. IV F. At $R=6.2a_0$ the $^1\Sigma_g^+(3p)$ and $^1\Sigma_g^+(3d)$ FO curves are no longer nearly degenerate, as they were for very large R and the Rydberg orbital of $^1\Sigma_g^+(5p\sigma, 3p)$ is dominated by $3d\sigma$ character. Near $R=4.2a_0$, the Rydberg orbital mixes in some $4f\sigma$ character [compare with $^1\Sigma_g^+(4f\sigma, 3s)$ at $R=3.0a_0$ in Fig. 11]. At $R=3.4a_0$, $4p\sigma$ character becomes evident, as expected. For smaller R this character is lost to the lower states, and the wave function must incorporate character from $^1\Sigma_g^+(5f)$ or $^1\Sigma_g^+(5p)$ (or higher states) in order to have an attractive core and fall below the ion curve, $^2\Sigma_u^+$. Near $R=2.6a_0$,

$^1\Sigma_g^+(5p\sigma, 3p)$ obtains repulsive character from the FO $^1\Sigma_g^+(2s)$ state. For smaller R, $5p\sigma$ character becomes evident in the Rydberg orbital, and the SCF potential curve follows the inner wall of an FO curve corresponding to $^1\Sigma_g^+(5p)$.

For $^1\Sigma_u^+(4s\sigma, 3p)$ near $R = 4.2a_0$ (see Figs. 8 and 12), the potential curve begins to rise as it obtains unfavorable core character from $^1\Sigma_u^+(3p)$. At smaller R it approaches the repulsive FO curve for $^1\Sigma_u^+(2p)$ and rises even further. Near $R = 2a_0$, favorable $4s\sigma$-like character causes the potential curve to drop.

For both of these states the basis set used is inadequate near R_e and one must include atomic functions with $n \geq 4$ in order to obtain a reasonable description.

Further details[16] of these calculations are discussed elsewhere, including a more quantitative description of the variation of the core-core interaction with R and an analysis of the Rydberg-core interaction in terms of the exchange kinetic energy.

V. NUMERICAL RESULTS AND COMPARISON WITH PREVIOUS WORK

The aim of the work described here has been to obtain a physical understanding of the excited states of He_2. Thus the emphasis has not been on obtaining quantitative accuracy for all of the excited states. Nevertheless, the basis set provides for a near-quantitative description of the lower excited states at large R (in the region of the maxima).

We find the magnitude of the maximum in the $A\,^1\Sigma_u^+(2s\sigma, 2s)$ state to be 0.0606 eV at $R = 5.82a_0$. Assuming the atomic contribution to the correlation energy to remain nearly constant for $R > 5.8a_0$, our calculated value for the magnitude of the maximum is probably 10 to 20% too large. From the spectra of Tanaka and Yoshino,[3] Sando and Dalgarno[21b] determined a potential for the A state and found a hump height of 0.049 ± 0.01 eV at $R = 5.86a_0$. In addition, their curve is quite broad in the vicinity of the maximum, in agreement with the curve calculated here. Recent results[10] for differential cross sections (describing the scattering of He* by He) obtained from the C- and A-state potentials calculated here show excellent agreement with the experimental results[9b] if the calculated potential curves are scaled so as to decrease the potential maximum in the A state by about 15%. Table III lists the results of the best previous theoretical calculations and experimentally derived results for the positions of extrema in the potential curves. Some comparisons to previous results have been discussed in Ref. 22.

While the results for the A-state maximum calculated here are in excellent agreement with experimentally derived results, we note that previous *ab initio* values for the maximum in the A state have all been too large (see Table III). We found that in order to obtain a good description of the maximum in the potential curve of the A state it is necessary that the basis include $2p\sigma$ functions that allow the $2s$ orbital to polarize properly away from the other He atom.

The SCF value for D_e $[D_e = E(R = \infty) - E(R = R_e)]$ of the A state is 1.883 eV ($R_e = 2.07a_0$), which is 75% of the experimentally derived value of 2.50 eV[2b] ($R_e = 1.96a_0$).[23] Reference 16 contains a discussion of the error in D_e and how it is related to the details of the basis set expansion of the orbitals.

The calculated maximum in $C\,^1\Sigma_g^+(2p\sigma, 2s)$ is 0.2166 eV at $R = 3.90a_0$. The calculated minimum is at $2.17a_0$, with $D_e = 0.6444$ eV. As for the A state we expect the calculated magnitude of the maximum to be about 10 or 20% too high, while the value for D_e may be too small by up to 0.6 eV.

Ginter[23] has reported 11 bands arising from the $C \rightarrow A$ transition and finds $R_e = 2.072\ a_0$ for the C state (about 5% smaller than the value found here). He also reports the emission spectra to only $v' = 5$ in the C state and suggests that the similar $c\,^3\Sigma_g^+$ state predissociates by $v' = 5$ or 6. This would imply the possibility of a small D_e for the C state (compared to the A state) in qualitative agreement with the results reported here.

Several previous calculations[20, 24] on the $C\,^1\Sigma_g^+$ state led to a totally repulsive curve because the $2s\sigma$ Rydberg orbital could not mix in $2p\sigma$ character and the avoided crossing could not occur. Only one previously reported calculation[25] has allowed for the avoided crossing in the upper state, thereby obtaining a maximum. However the wave functions used provided only a minimal description and led to a large value (0.7 eV) for the hump.

In discussing their experimentally determined potential curves Ginter and Battino[26] did not correlate the He $(1s^2; {}^1S)$ + He $(1s, 2p; {}^1P)$ separated-atom limit with any $^1\Sigma_g^+$ molecular state at R_e. Nevertheless they speculated that it might correlate with a state denoted as $4p\sigma\,^1\Sigma_g^+$. This is the first state found above those that correlate with the other $n = 2$ separated atom levels and was estimated to have its $v = 0$ level at several hundred cm^{-1} below the above $R = \infty$ limit. Thus the identification of our $^1\Sigma_g^+(3p\sigma, 2p)$ state as Ginter's $4p\sigma$ state appears to be very reasonable although the Rydberg orbital is $3p\sigma$-like. (We find that the higher $^1\Sigma_g^+(4p\sigma, 3d)$ state has $4p\sigma$ character.)

Near $R = 2.2a_0$ the SCF-GVB $D\,^1\Sigma_u^+(3s\sigma, 2p)$ and $F\,^1\Sigma_u^+(3d\sigma, 3s)$ states become nearly degenerate (see Fig. 8). In Ref. 26 at large R, these states are allowed to cross, and as a result, for separa-

tions greater than the crossing point, our states are equivalent to the F and D states, respectively, of Ref. 26. In qualitative agreement with the calculations presented here, Ginter's $f\,^3\Sigma_u^+$ state (which should be similar to the corresponding singlet state $F\,^1\Sigma_u^+$) shows a large maximum at about $R=3.1\ a_0$. Near $R=2.7\ a_0$ his F state crosses the D state with the minimum of the D state falling about 700 cm^{-1} below that for the F state. (Our calculated $D\,^1\Sigma_u^+(3s\sigma, 2p)$ lies 410 cm^{-1} below $F\,^1\Sigma_u^+$ $(3d\sigma, 3s)$ at the minimum.) From the noncrossing rule we know that SCF-GVB Born-Oppenheimer curves for these states will not cross. However from Fig. 11 we see that the Rydberg orbitals for the $^1\Sigma_u^+(3s\sigma, 2p)$ and $^1\Sigma_u^+(3d\sigma, 3s)$ states switch character near $R=2.2a_0$. This suggests that we use the diabatic curves. Inclusion of nuclear kinetic energy will tend to mix these nearly degenerate (Born-Oppenheimer) GVB states. Probably a better set of zero-order states for describing dynamic processes would be the diabatic states in which (for $R<3a_0$) one state is taken as having $3d\sigma$ character and the other as having $3s\sigma$ character. The calculated R_e for $D\,^1\Sigma_u^+(3s\sigma, 2p)$ is $2.17a_0$, which agrees favorably with the experimentally derived value of $2.02a_0$.[27] There are no accurate experimentally derived data in the literature for D_e or the magnitude and position of the maximum.

The similarity in the shape of the potential wells for $F\,^1\Sigma_u^+(3d\sigma, 3s)$ and $A\,^1\Sigma_u^+(2s\sigma, 2s)$ has been discussed in Sec. IV. For the former state we find $D_e=1.862$ eV compared to 1.883 eV for the A state. The calculated R_e for $F\,^1\Sigma_u^+(3d\sigma, 3s)$ is 2.19 a_0 compared to the experimental value of $2.06a_0$.[28] Also we find that there is a small maximum of $0.00015h$ in the calculated potential curve (cubic spline fitted) at $R=11.38$ to $11.54a_0$ (see Table III). This arises from the unfavorable overlap of the outer maximum of the Rydberg orbital with the core orbitals on the opposite center and has been discussed in Secs. III and IV. Tanaka and Yoshino[3,29] have reported a band in absorption at 540.77 Å corresponding to an energy slightly greater than the atomic line, $1s3s\,^1S \leftarrow 1s^2\,^1S$ (540.94 Å). They also report that this band was quite similar in appearance to the band at 600 Å, which is due to transitions from the ground state to the quasibound levels (occurring at energies between the maximum and the $R=\infty$ asymptote) of the A state. As a result they proposed that $F\,^1\Sigma_u^+(3d\sigma, 3s)$ has a hump of about 60 cm^{-1} or 0.000 27 hartree.

There is little quantitative information in the literature describing the potential curves of the higher states reported here. Table III contains a summary of the locations and magnitudes of the maxima and minima in the SCF-GVB curves.

From the analysis presented in Secs. III and IV one would expect the FO curves for $^{1,3}\Pi_g(2p)$, $^{1,3}\Pi_g(3p)$, and $^{1,3}\Pi_u(3d)$ to be attractive at small R while $^{1,3}\Pi_u(2p)$, $^{1,3}\Pi_u(3p)$, and $^{1,3}\Pi_g(3d)$ will be repulsive at small R, with all the curves showing no unfavorable (Pauli-principle-induced) maxima at large R since $\lambda_2=0$. The latter three states should have large maxima in the SCF curves resulting from avoided crossings with attractive higher states of the same symmetry. Thus a large maximum in $^{1,3}\Pi_u(3d\pi, 2p)$ would arise from the crossing of $^{1,3}\Pi_u(2p)$ with $^{1,3}\Pi_u(3d)$. These predictions have been confirmed for the $^{1,3}\Pi_u$ states by the CI calculations of Gupta and Matsen[30] and Browne[31] and for $^1\Pi_g(2p\pi, 2p)$ and $^1\Pi_u(3d\pi, 2p)$ by Gupta *et al.*[32]

VI. BUBBLES IN LIQUID HELIUM

Walters and co-workers[7] have found that particle bombardment on liquid helium leads to excited states of He and He_2, and they have examined the spectroscopy of these states. Interpretation of the results[7a,8] suggests that each excited state leads to a bubble radius[8b] of $12a_0 \approx 6\frac{1}{2}$ Å (for He $2\,^3S$) or larger. The origin of the bubble around an excited-state atom is the same as the origin of the barriers in the He_2^* potential curves, namely, the repulsive interaction arising from the Pauli principle. The excited state has a much more diffuse orbital so that these repulsive effects have a much larger range than between ground-state atoms. Since the effect involves basically the overlap of a ground-state atom with the excited orbital, the size and shape of the bubble should be closely related to the size and shape of the excited orbital.

From Fig. 11 we see that the $2s\sigma$ orbital of the $A\,^1\Sigma_u^+$ state is essentially identical in size and shape to the $2s$ orbital of He $2\,^1S$. Thus the bubbles should be essentially identical for these two cases. The best estimate[8b] for the bubble involving the $2s$ orbital of He $2\,^3S$ is a diameter of $24a_0=12\frac{1}{2}$ Å. This compares with a diameter of $18\frac{1}{2}a_0$ for the outer contour (0.005 a.u.) in Fig. 11. In order to provide some idea of the shapes of the bubbles expected for the other excited states of He* and He_2^*, we will scale the size found by the 0.005-a.u. contour so as to obtain $24a_0$ for He $2\,^1S$. For $C\,^1\Sigma_g^+$ this leads to $17\times12\frac{1}{2}$ Å. This state has the shape of a $2s$ orbital ($12\frac{1}{2}\times12\frac{1}{2}$ Å) at $R=\infty$ but the shape of a $2p\sigma$ orbital at small R. The next two states, $^1\Sigma_u^+(3s\sigma, 2p)$, $^1\Sigma_g^+(3p\sigma, 2p)$, correlate with $2p$ at $R=\infty$ ($13\frac{1}{2}\times10$ Å) but are much larger at R_e ($20\frac{1}{2}\times16$ Å for $3s\sigma$ and $26\times17\frac{1}{2}$ Å for $3p\sigma$). (Note that except for the A and C states, the 0.005-a.u. contour is the *second* one.) The next two states, $^1\Sigma_u^+(3d\sigma, 3s)$ and $^1\Sigma_g^+(4f\sigma, 3s)$, correlate with $3s$ at $R=\infty$ (size $19\times17\frac{1}{2}$ Å) and are only slightly larger at

R_e (20×19 Å for $3d\sigma$ and $23\frac{1}{2}\times17\frac{1}{2}$ Å for $4f\sigma$).

The envelope of the rotational structure of the emissions from $d^3\Sigma_u^+$ and $D^1\Sigma_u^+$ is preserved in liquid helium, suggesting unusually long vibrational and rotational lifetimes for a liquid. From the roughly spherical shape of the $3s\sigma$-like orbital of the $D^1\Sigma_u^+$ state (Fig. 11), long relaxation times are not unexpected.

VII. SUMMARY

In conclusion we find that the independent-particle nature of the projected G1 or GVB wave functions leads to a highly interpretable and meaningful description of the excited states of He_2. Two types of interactions have been shown to be important in understanding the shapes of the potential energy curves: Interaction between core orbitals on opposite centers is dominant at small R whereas at large R the significant interaction is between Rydberg and core orbitals on opposite centers. The former interaction leads to repulsive and attractive FO potential energy curves which in turn helps us to describe avoided crossings of SCF curves. At large R, where spatial projection is not important, we have found that the unfavorable Rydberg-core interactions can be understood in terms of the Pauli principle and indeed the unfavorable maxima can be quite large [e.g., see $^1\Sigma_g^+(3p\sigma, 2p)$ and $^1\Sigma_u^+(3s\sigma, 2p)$]. These ideas can also be used to help understand the shapes of potential curves for both heteronuclear and homonuclear diatomics containing other rare gas atoms. Calculations[33] on Ne_2 have shown the usefulness of these ideas. Furthermore the results presented here for He_2 imply that the experimentally derived[34] barrier in $He(2^3s)+Ne(2p^6)$ is Pauli principle induced. Other molecules having repulsive ground states (e.g., diatomics from Group II of the Periodic Table) may also be amenable to the ideas discussed here. Such an application has already been made to Hg_2.[35] Lastly we note that it has also been shown[36] that the rotational barriers about single bonds (e.g., C_2H_6 and CH_3OH) also arise directly from the Pauli-principle-induced repulsion of singlet coupled pairs of orbitals.

ACKNOWLEDGMENTS

The authors wish to thank Dr. D. L. Huestis, Dr. R. C. Ladner, Dr. T. H. Dunning, and Dr. R. J. Blint for many informative conversations and for the use of their computer programs and subroutines.

APPENDIX: UPPER BOUNDS FROM GVB WAVE FUNCTIONS

By requiring the energy for the GVB singlet wave function

$$\Psi = N(\phi_a\phi_b + \phi_b\phi_a)(\alpha\beta - \beta\alpha) \tag{A1}$$

to be stationary under first-order variations in the orbitals ϕ_a and ϕ_b, we obtain the GVB equations

$$H_a\phi_a = \epsilon_a\phi_a, \tag{A2}$$

$$H_b\phi_b = \epsilon_b\phi_b, \tag{A3}$$

where H_a and H_b are one-electron Hamiltonian operators and ϵ_a and ϵ_b are orbital eigenvalues. By choosing a basis for χ_μ such that $\langle\chi_\mu|\phi_b\rangle = 0$, Eq. (A3) can be written equivalently[15] as

$$\langle\chi_\mu|H_b|\phi_b\rangle = \langle\phi_a\chi_\mu|\mathcal{H} - E|\phi_a\phi_b + \phi_b\phi_a\rangle = 0, \tag{A4}$$

where $\mathcal{H}$ is the total Hamiltonian and E is the total energy. To solve for the first excited state described by (A1), we solve self-consistently for the lowest solution of Eq. (A2) (ϕ_{1a}) and the second solution of Eq. (A3) (ϕ_{2b}), yielding the equations

$$\begin{aligned} H_a\phi_{1a} &= \epsilon_{1a}\phi_{1a}, \\ H_b\phi_{2b} &= \epsilon_{2b}\phi_{2b}. \end{aligned} \tag{A5}$$

Let ϕ_{1b} be the first solution of H_b,

$$H_b\phi_{1b} = \epsilon_{1b}\phi_{1b}, \tag{A6}$$

and consider the two wave functions

$$\begin{aligned} \psi_1 &= N_1(\phi_{1a}\phi_{1b} + \phi_{1b}\phi_{1a})(\alpha\beta - \beta\alpha), \\ \psi_2 &= N_2(\phi_{1a}\phi_{2b} + \phi_{2b}\phi_{1a})(\alpha\beta - \beta\alpha). \end{aligned} \tag{A7}$$

From the Hylleraas-Undheim-MacDonald theorem[37] we know that the lowest state of the wave function

$$\Phi_i = C_{1i}\psi_1 + C_{2i}\psi_2 \tag{A8}$$

has an energy which is an upper bound on the exact energy of the ground state and that the energy of the second state of (A8) is an upper bound on the exact energy of the second singlet state. We make use of this theorem by taking $\chi_\mu = \phi_{1b}$ and rewriting (A4) as

$$\langle\phi_{1a}\phi_{1b}|\mathcal{H} - E|(\phi_{1a}\phi_{2b} + \phi_{2b}\phi_{1a})\rangle = 0 \tag{A9}$$

since $\langle\phi_{1b}|\phi_{2b}\rangle = 0$. But (A9) is just

$$\langle\psi_1|\mathcal{H} - E|\psi_2\rangle = 0. \tag{A10}$$

Therefore (A10) implies that the solutions to (A8) are

$$\Phi_1 = \psi_1, \quad \Phi_2 = \psi_2.$$

Thus the GVB solution for the $2\,^1S$ state leads to an energy that is an upper bound on the exact energy of the $2\,^1S$ state. (Note that here we have constructed ψ_1 using ϕ_{1a}, which was solved for self-

consistently in the field due to ϕ_{2b}. While ψ_1 is not the optimum description of the ground state, we need only assume it to be lower in energy than ψ_2 in order to complete the above proof.)

Now consider the HF wave function, which has the form (A1) except that ϕ_a and ϕ_b are required to be orthogonal. In this case (A2) and (A3) become

$$H_a^{\mathrm{HF}}\phi_a = \epsilon_a\phi_a + \epsilon_{ab}\phi_b ,$$

$$H_b^{\mathrm{HF}}\phi_b = \epsilon_b\phi_b + \epsilon_{ba}\phi_a ,$$

where ϵ_{ab} and ϵ_{ba} are Lagrange multipliers. Thus (A4) becomes

$$\langle\chi_\mu | H_b^{\mathrm{HF}} | \phi_b\rangle = \langle\phi_a\chi_\mu | \mathcal{H} - E | \phi_a\phi_b + \phi_b\phi_a\rangle$$

$$= \epsilon_b\langle\chi_\mu | \phi_b\rangle + \epsilon_{ba}\langle\chi_\mu | \phi_a\rangle . \qquad \text{(A11)}$$

Now taking $\chi_\mu = \phi_a$ and

$$\psi_1 = N_1(\phi_a\phi_a)(\alpha\beta - \beta\alpha) ,$$

$$\psi_2 = N_2(\phi_a\phi_b + \phi_b\phi_a)(\alpha\beta - \beta\alpha) ,$$

in (A8), we obtain for (A11)

$$\langle\psi_1 | \mathcal{H} - E | \psi_2\rangle = \epsilon_{ba} \neq 0 .$$

Therefore ψ_2 is not a solution of (A8) and the Hylleraas-Undheim-MacDonald theorem[37] does not apply. Indeed the calculated HF energy for He ($2\,^1S$) falls below the experimental value for the second state as shown in Table I. As pointed out in the text, the form of ψ_2 is inconsistent with the form of the HF wave functions for the other $n=2$ excited states. The proper form, shown in (3′), is equivalent to the GVB wave function and does lead to an upper bound on the exact $2\,^1S$ energy.

In a manner analogous to that used above for wave functions (A7), we can show that the four-electron projected SCF-GVB wave function for the nth excited state of He_2 also leads to an upper bound to the exact energy of the nth state of the same symmetry. Note that the orbitals from FO-GVB calculations are not solutions of Eq. (A5) (except at $R=\infty$) and as a result the energy of the FO wave functions need not be upper bounds to the exact energy.

---

†Partially supported by Grants Nos. GP-15423 and GP-40783X from the National Science Foundation. Based on the Ph.D. thesis (California Institute of Technology, 1972) of S. L. Guberman.

*Current address: Center for Astrophysics, Harvard College Observatory and Smithsonian Astrophysical Observatory, Cambridge, Mass. 02138.

[1](a) R. A. Buckingham, Trans. Faraday Soc. 54, 453 (1958); (b) Y. Tanaka, K. Yoshino, and D. E. Freeman, J. Chem. Phys. 59, 5160 (1973).

[2](a) K. M. Sando, Mol. Phys. 21, 439 (1971); (b) 23, 413 (1972); (c) A. L. Smith, J. Chem. Phys. 49, 4817 (1968); (d) B. Liu, Phys. Rev. Lett. 27, 1251 (1971).

[3]Y. Tanaka and K. Yoshino, J. Chem. Phys. 50, 3087 (1969).

[4]R. E. Huffmann, Y. Tanaka, and J. C. Larrabee, Appl. Opt. 2, 617 (1963); J. Opt. Soc. Am. 52, 851 (1962); Y. Tanaka, A. S. Jursa, and F. J. LeBlanc, *ibid.* 48, 304 (1958).

[5]N. G. Basov, V. A. Danilychev, and Yu. M. Popov, Sov. J. Quantum Electron. 1, 18 (1971); H. A. Koehler, L. J. Ferderber, D. L. Redhead, and P. J. Ebert, Appl. Phys. Lett. 21, 198 (1972); E. V. George and C. K. Rhodes, *ibid.* 23, 139 (1973); Physics Today 26 (No. 8), 17 (1973).

[6]J. Nuckolls, J. Emmett, and L. Wood, Physics Today 26 (No. 8), 46 (1973).

[7](a) W. S. Dennis, E. Durbin, Jr., W. A. Fitzsimmons, O. Heybey, and G. K. Walters, Phys. Rev. Lett. 23, 1083 (1969); (b) J. C. Hill, O. Heybey, and G. K. Walters, *ibid.* 26, 1213 (1971).

[8](a) A. P. Hickman and N. F. Lane, Phys. Rev. Lett. 26, 1216 (1971); (b) J. P. Hansen and E. L. Pollock, Phys. Rev. A 5, 2214 (1972).

[9](a) R. A. Buckingham and A. Dalgarno, Proc. R. Soc. Lond. A213, 506 (1952); F. D. Colgrove, L. D. Schearer, and G. K. Walters, Phys. Rev. 135, A353 (1964); V. Sidis and H. Lefebvre-Brion, J. Phys. B 4, 1040 (1971); E. W. Thulstrup and H. Johansen, Phys. Rev. A 6, 206 (1972); H. J. Kolker and H. H. Michels, J. Chem. Phys. 50, 1762 (1969); (b) H. Hoberland, C. H. Chen, and Y. T. Lee (unpublished).

[10]B. B. Andresen and A. Kuppermann (unpublished).

[11]C. E. Moore, *Atomic Energy Levels* (U. S. GPO, Washington, D. C., 1949), Vol. I.

[12](a) W. A. Goddard III and R. C. Ladner, J. Am. Chem. Soc. 93, 6750 (1971); (b) The overlaps for the $1\,^1S$ and $2\,^1S$ core orbitals are (with all orbitals on the same center), $\langle\phi_{1s}|\phi_{1s'}\rangle = 0.879$, $\langle\phi_{1s}|\phi_{\overline{1s}}\rangle = 0.996$ and $\langle\phi_{1s'}|\phi_{\overline{1s}}\rangle = 0.910$.

[13]W. A. Goddard III, Phys. Rev. 176, 106 (1968).

[14]W. J. Hunt, W. A. Goddard III, and T. H. Dunning, Chem. Phys. Lett. 6, 147 (1970).

[15]For a discussion of spatially unprojected G1 wave functions see W. A. Goddard III, Phys. Rev. 157, 73 (1967); 157, 81 (1967).

[16](a) For a discussion of the projected G1 wave functions used here see S. L. Guberman, Ph.D. thesis (California Institute of Technology, 1972); (b) S. L. Guberman and W. A. Goddard III (unpublished).

[17]W. J. Hunt, P. J. Hay, and W. A. Goddard III [J. Chem. Phys. 57, 738 (1972)] use the term GVB to describe somewhat restricted spatially unprojected wave functions containing strong orthogonality constraints between orbitals. In our work we make no orthogonality constraints whatsoever between any orbitals.

[18](a) Note that for small R, $\phi_{vr} \approx \phi_{vl}$ for s, d, etc., orbitals while $\phi_{vr} \approx -\phi_{vl}$ for p, f, etc., atomic orbitals. (b) With Eq. (9) we obtain for the total wave function

$$\Psi = \mathcal{A}\{[(\phi_{cl}\phi_{cl'} + \phi_{cl'}\phi_{cl})(\phi_{\bar{cr}}\phi_{vr} + \phi_{vr}\phi_{\bar{cr}}) \pm (\phi_{cr}\phi_{c'r} + \phi_{c'r}\phi_{cr})(\phi_{\bar{cl}}\phi_{vl} + \phi_{vl}\phi_{\bar{cl}})]\alpha\beta\alpha\beta\}$$

$$= \mathcal{A}\{[(\phi_{cl}\phi_{c'l} + \phi_{c'l}\phi_{cl})\varphi_{\bar{cr}} \pm (\phi_{cr}\phi_{c'r} + \phi_{c'r}\phi_{cr})\phi_{\bar{cl}}]\phi_v\alpha\beta(\alpha\beta - \beta\alpha)\},$$

and hence Fig. 6(a) contains core interactions as in Fig. 6(b). (c) For a triplet excited state only the spin function in the last equation of (b) is changed. (d) For $^1\Sigma_u^+(2s)$ at $R=\infty$ this is the lowest state of this symmetry and as a result the Rydberg orbital need not have any radial nodes. However, for $^1\Sigma_g^+(2s)$ at $R=\infty$ this is the second state of this symmetry and the Rydberg orbital has one radial node. Thus the Rydberg orbitals [see Fig. 1(b)] for these two states are similar at large r but differ near $r=0$. The differences come at small enough r to have no effect on the discussion here. Nevertheless this also leads to a slight difference in the calculated *molecular* energies at $R=\infty$ (0.02 eV in the above states) which is again small enough so that it can be neglected in the qualitative discussion. Similar splittings, of even smaller magnitude, occur for the states having Rydberg orbitals $\phi_v = 3s$ and $\phi_v = 3d$. For $\phi_v = 2p$, $3p$ the Rydberg orbitals are orthogonal by symmetry to the lower orbitals and such splittings do not arise. See Ref. 16 for a more detailed discussion. (e) See Refs. 2–4, 16, 19–26, 28, and 29 and references cited therein.

[19]R. S. Mulliken, Phys. Rev. 136, A962 (1964).

[20]R. A. Buckingham and A. Dalgarno, Proc. R. Soc. Lond. A213, 327 (1952). These authors point out that maxima in potential curves can arise from the overlap of wave functions of separate atoms.

[21](a) The slight distortion of the $3s$ and $3d$ Rydberg orbitals at $R=\infty$ in Figs. 11 and 12 is due to the incomplete description of the $3d$ orbital used here and does not affect the qualitative discussion. Only a contracted Gaussian-type $3d_{z^2}$ function was included for polarization and the description of the $3d\sigma$ orbital. (b) K. M. Sando and A. Dalgarno, Mol. Phys. 20, 103 (1971).

[22]S. L. Guberman and W. A. Goddard III, Chem. Phys. Lett. 14, 460 (1972).

[23]M. L. Ginter, J. Chem. Phys. 42, 561 (1965).

[24]D. C. Allison, J. C. Browne, and A. Dalgarno, Proc. Phys. Soc. 89, 41 (1966).

[25]J. C. Browne, J. Chem. Phys. 42, 2826 (1965).

[26]M. L. Ginter and R. Battino, J. Chem. Phys. 52, 4469 (1970).

[27]*Donnees Spectroscopiques Relatives aux Molecules Diatomiques*, edited by B. Rosen (Pergamon, Oxford, 1970).

[28]M. L. Ginter, J. Chem. Phys. 45, 248 (1966).

[29]Y. Tanaka and K. Yoshino, J. Chem. Phys. 39, 3081 (1963).

[30]B. K. Gupta and F. A. Matsen, J. Chem. Phys. 50, 3797 (1969).

[31]J. C. Browne, Phys. Rev. 138, A9 (1965).

[32]B. K. Gupta, E. M. Greenawalt, C. E. Rodriguez, D. R. Scott, P. L. M. Plummer, J. C. Browne, and F. A. Matsen, Bull. Am. Phys. Soc. 12, 182 (1967).

[33]J. Cohen and B. Schneider (unpublished).

[34]R. Arrathoon, Phys. Rev. Lett. 30, 469 (1973).

[35]D. J. Eckstrom, R. A. Gutcheck, R. M. Hill, D. L. Huestis, and D. C. Lorents, Stanford Research Institute Report No. MP73-1, 1973 (unpublished).

[36]O. J. Sovers, C. W. Kern, R. M. Pitzer, and M. Karplus, J. Chem. Phys. 49, 2592 (1968); C. W. Kern, R. M. Pitzer, and O. J. Sovers, *ibid.* 60, 3583 (1974).

[37]E. Hylleraas and B. Undheim, Z. Phys. 65, 759 (1930); J. K. L. MacDonald, Phys. Rev. 43, 830 (1933).